Silk Bone Screws and Plates as a Novel Fracture Fixation Device

A thesis submitted by

Gabriel S. Perrone

In partial fulfillment of the requirements for the degree of

Master of Science

In

Biomedical Engineering

TUFTS UNIVERSITY

May 2013

Advisor: David L. Kaplan

Abstract

Because current resorbable fracture fixation devices experience problems with implantation technique and negative host response, there is a need for new devices that have multifunctional features. These include immediate fracture stabilization upon implantation, complete degradation to avoid need for hardware removal, robust mechanical properties to allow for implantation, and ability to resterilized and reused to save on costs. The goal of this study was to prepare and characterize a new family of resorbable screws and plates from silk protein for craniomaxillofacial (CMF) repair. The screws and plates were prepared using a solvent-based process, treated with methanol to induce crystalline, beta sheet structures for stability then machined to the desired geometries. The silk material was evaluated in dry and in hydrated environments to mimic implantation as well as *in vivo* fixation conditions. The silk biomaterials compared favorably with the mechanical properties of current poly-lactic-co-glycolic acid (PLGA) resorbable fixation systems, while offering a number of advantages including ease of implantation, conformal fit to the repair site, easy sterilization by autoclaving and non-inflammatory response. Assessment of the screws *in vivo* in a rat femur model showed they were self-tapping, remained fixed in the bone for a 4 week trial, exhibited biocompatibility, and showed signs of normal bone remodeling. These silk screws and plates exhibit potential for resorbable fixation systems due to their mechanical strength, ease of implantation, ability to degrade, tunable properties with autoclaving, and potential to be resterilized and reused if opened but not used in the operating room.

Acknowledgements

I would like to thank my thesis committee Dr. David Kaplan, Dr. Gary Leisk, and Dr. Fiorenzo Omenetto for their support and motivation to pursue this exciting research. I would also like to thank Dr. Samuel Lin and Dr. Ahmed Brahim of Beth Israel Deaconess Medical Center for their assistance on the clinical needs, and passion for this research. This project was funded by the Tissue Engineering Resource Center (TERC) (NIH P41 EB002520).

I wish to thank Mike Ryan and Patrick Hughes from Synthes for providing the surgical drill and attachments, Tiger Tao for assistance with the SEM, Ben Partlow for running FTIR, Roberto Elia for general experimental advice, Vinnie Miraglia for help with hardness testing, Sharon Fox for histological characterization, and Jodie Moreau for assistance and guidance with the animal studies. Last but certainly not least, I wish to thank Tim Lo and Bernke Papenburg for their endless support, motivation, and knowledge.

A special thanks to Rosie for helping with thesis graphics, all of 200 Boston Ave., Geoffrey Brahmer, Nereus for providing endless amusement, Ethan Golden for life advice and fish tank service, Jodie for homemade cookies, and Ben Partlow for showing us all how to be optimistic. Finally, I would like to thank my parents and family for giving me the opportunity to perform such amazing research and supporting me in everything I do.

Table of Contents

List of Figures

List of Tables

List of Equations

1. Introduction

1.1 Problem statement

Because current resorbable devices experience problems with implantation technique and negative host response, there is a need for new devices that have multifunctional features. These include immediate fracture stabilization upon implantation, complete degradation to avoid need for hardware removal, robust mechanical properties to allow for implantation, and ability to be resterilized and reused to save on costs. The new silk devices will be tailored for craniomaxillofacial (CMF) reconstruction.

1.2 Background

1.2.1 Craniomaxillofacial complex

The new devices will be targeted towards the CMF complex which consists of the anatomical area of the mouth, jaws, face, and skull. This is the target application area due to the nature of fracture fixations in the CMF complex. Most fracture fixations are non-load bearing and, thus, can be fixed with weaker, less stiff resorbable devices. Further, current resorbable devices are only currently used in pediatric CMF procedures so the new silk devices will be tailored for this application for comparison.

1.2.2 History

Plate fixation of fractures was first pioneered by Dr. Carl Hansmann in Germany in the middle to late 1880s [1, 2]. However, these systems were not routinely

implemented until modern medical technology such as antibiotics, advances in germ theory, anesthesia, antisepsis, and modern materials resistant to corrosion became available [1, 2]. Robert Danis declared the routine use of plate fixation for traumatology procedures in 1949. Self-locking compression plates with tapered screw heads (mandibularcompression-screw [MCS] plates) and eccentric plate bore-holes were developed in the 1960s and are still used today. Common materials used for CMF procedures included stainless steel and vitallium, an alloy composed of cobalt, chrome and molybdenum. However, in 1983, Brane-mark outlined the superiority of titanium over other metals in terms of biocompatibility and mechanical properties. Biodegradable plates and screws became available during the mid-1990s. [2]

1.2.3 Current fixation device systems

Approximately 3 million facial injuries occur annually. The American Society of Plastic Surgeons reported over 200,000 CMF surgical procedures in 2012 which is a 164% increase from 2000 and a 7% increase from 2011[3]. The Millennium Research Group reported that the US market for trauma devices (including metallic plates and screws, intramedullary (IM) nails, cannulated screws, conventional hip screws, ancillary trauma devices, external fixation devices, and long-bone growth stimulation devices) experienced moderate expansion during 2011 [4]. The market for CMF devices in the US (which includes plate and screw fixation, bone graft substitutes (BGS), cranial flap fixation devices, CMF distraction devices, and temporomandibular joint (TMJ) replacement devices) is

expected to continue to experience strong growth. Despite the current economic setting, this growth will be sustained as a result of the non-elective nature of trauma procedures (motor vehicle accidents, sports-related fractures), and improved detection and treatment of brain lesions. In addition, the ongoing United States military involvement abroad results in soldiers sustaining CMF and extremity injuries. Therefore, the availability of a reliable biodegradable device system that is a mechanical and conformational match to CMF needs and also compatible, would be useful for CMF surgery. Plate exposure of metallic devices following open reduction and internal fixation may pose additional reconstructive challenges and risks. Biodegradable plating systems that hold fracture segments in place while degrading over time may therefore be clinically significant.

1.2.4 Metal systems

1.2.4.1 Overview

Currently, a wide variety of fixation systems are available including miniplates, microplates, meshes, and screws (Figure 1) [2]. Metal systems are typically made of titanium and provide for an accessible implantation technique as the screws are self-tapping and only require pre-drilling of a pilot hole. In addition, the plates can be shaped/adjusted intra-operatively due to the ductility of metal. The systems can be resterilized and reused due to sustained mechanical integrity, measured by maximum flexure before fracture, even after 50 cycles of autoclaving [2, 5]. Resterilization and reuse refers to device systems that were opened in the

operating but never implanted into a patient, and, thus, can be reused once they are resterilized.

Figure 1 – Examples of metallic bone screws and plates from Synthes MatrixMIDFACE Plating System.

Despite the widespread use of metallic screws and plates for bone fixation, one of their disadvantages includes extreme stiffness causing stress shielding; bone remodels based on the loads it is placed under and, thus, bone cannot properly remodel if the implant is bearing most of the load. Other potential problems during the fracture healing phase include potentially poor wound healing and plate exposure, wound dehiscence, temperature sensitivity, palpability, device migration, pain, infection, surrounding soft tissue infection, growth disturbance in children in up to 50% of pediatric cases [6], and renal failure due to accumulation of corrosion products. All of these issues warrant removal of metallic implants [1, 2, 7-10]. The most common causes of device removal are infection, pain, and exposure with removal rates ranging approximately from 4 – 12% [1, 2]. In

general, when opting to use a metallic device, roughly 10% of patients will require a second operation for hardware removal [1].

While other titanium implants such as pacemakers and articular implants remain inside the patient and maintain function, titanium fixation systems are effectively functionless once fracture healing is complete. Asymptomatic plate and screw removal after complete fracture healing is subject to controversy due to lack of scientifically founded indications or contraindications [2]. The negative outcomes of plate removal are hospital acquired infection (HAI), increased recovery time and cost due to multiple surgeries and wound sites. However, fixation systems after fracture healing is complete are removed for various reasons. Plates are removed due to risk of infection associated with protrusion of screws into the nasal sinuses; this may allow the potentially contaminated mucosa an infection-duct enabling bacterial diffusion. Titanium ions can enhance implant directed bone-resorption by activation and secretion of cytokines which can lead to infection. Some systems are removed based on localization with respect to the sinus wall or alveolar ridge and always for children. Other reasons include patient request, radiological artifacts, limited radiological imaging or shielding for radiation therapy, palpability especially in thin skin cover areas, visibility, hardware loosening, thermal sensitivity, and even problems with regards to airport screening [1, 2, 10-15]. The removal of metallic plates and screws after fracture union following open reduction and internal fixation (ORIF) is also not free of complications and, thus, asymptomatic removal is controversial. The majority of

asymptomatic plates are not removed in the United States potentially for financial reasons.

1.2.4.2 Stainless steel and Cobalt Based Alloys

Metal alloys are the most popular materials used for fracture-fixation devices [7]. These metals include stainless steel, cobalt based alloys, and titanium. Stainless steel contains variable amounts of nickel, iron, chromium, manganese, vanadium and/or molybdenum and is extremely rigid creating difficulties with plate shaping and more susceptibility to surface damage and subsequent corrosion after shaping [1]. Corrosion can cause the formation of granulation tissue on the surface leading to sensitization. Further, stainless steel is stiffer than bone which leads to stress shielding; this can trigger bone resorption and weakening of the bone [2].

Vitallium is a cobalt-chromium-molybdenum based alloy that has twice the tensile strength, 50% more yield strength, and twice the hardness as some other metals, thus, allowing for thinner plates for fixation. However, like stainless steel, cobalt based alloys may lead to corrosion and production of charged ions which have negative secondary effects such as elevation and sometimes accumulation of metal ions in the blood [1, 2].

1.2.4.3 Titanium

Due to the problems with stress shielding and corrosion of both stainless steel and cobalt alloys, titanium is often utilized due to its biocompatibility and corrosion-

resistance. While the elastic modulus (stiffness) of titanium (105 GPa) is still well above the elastic modulus of bone (20 GPa), it is only half the modulus of stainless steel or cobalt alloys making the effects of stress shielding less likely. Despite titanium's decreased rigidity, it allows for more easily adaptable plates *in situ* [1]. Further, an approximately 10 micron thick layer of titanium-oxide forms spontaneously which is responsible for corrosion-resistance and for the adhesion of glycoproteins *in vivo*; glycoproteins are important in cell-cell interactions so their adhesion to titanium *in vivo* may allow for better remodeling of the defect than other metals. Bone is capable of binding to titanium so titanium has better osseointegration properties than other metals. While stainless steel screws may loosen over time, titanium screws become more fixed in the bone resulting in a higher release torque than insertion torque. Titanium devices are typically composed of alloys because pure titanium is expensive. Despite titanium's better corrosion resistance, corrosion can occur due to flexure under mechanical loads and also friction between screws and plates. Two common titanium alloys are Ti-6Al-4V (6% aluminum, 4% vanadium) or Ti-6Al-7Nb (6% aluminum, 7% niobium). Although titanium devices have decreased in price, they remain more expensive than their stainless steel counterparts. [1, 2]

While titanium has low toxicity in both ionic and particle form and is subject to renal excretion, rulite, a titanium corrosion product, can accumulate in the lymph nodes, liver, spleen, bone marrow and brain. Higher toxicity results from alloy additives such as aluminum ions and vanadium. Aluminum may accumulate in

patients with impaired renal function but this is typically noticed in hip implants rather than CMF applications. While toxicity concerns are valid, there have not been reported any clinically relevant toxicity levels due to titanium implants. Sensitization (allergic reaction) to titanium is rare and has not been reported for CMF applications but only for orthopedic applications and pacemaker implants. Animal tests show no carcinogenic indications and malignant tumors in surrounding tissues of titanium implants are pathogenically speculative. Currently, studies are inconclusive regarding the negative side effects of titanium remaining in the body for extended periods of time and, thus, provide little relevant information to surgeons. [1, 2]

1.2.5 Resorbable systems

1.2.5.1 Overview

Fracture stabilization by rigid internal fixation is only necessary until fracture healing is complete. Therefore, resorbable implants that degrade with time eliminate the need for functionless hardware removal. Figure 2 shows examples of a resorbable fixation system from Synthes; the plates can be cut and shaped to desired geometries *in situ*. Due to the disadvantages of metal implants such as necessity of a second operation for device removal, stress shielding, and thermal sensitivity, resorbable osteosynthesis systems have been utilized. Additionally, despite orthopedic fixation systems necessity of metallic devices capable of load bearing, CMF repair systems do not require the same rigidity and strength as the physiological forces are not as significant as in orthopedic repair; thus, weaker,

less stiff resorbable materials are acceptable for use in CMF repair. In the 1960s and 1970s, resorbable systems began development but it was not until the mid-1990s that resorbables became common place in clinical settings due to developments in biomaterials, biomechanics, and clinical experience. The materials for resorbable fixation systems are derived from readily available biodegradable suture materials. Most current resorbable systems are polyester, α-hydroxy acids composed of polylactic acid (PLA), polyglycolic acid (PGA) or poly-lactic-*co*-glycolic acid (PLGA). However, other polyester resorbable systems exist such as polycaprolactone, polyhydroxybutyrate, polytrimethylcarbonate, and polyurethane. [1, 2]

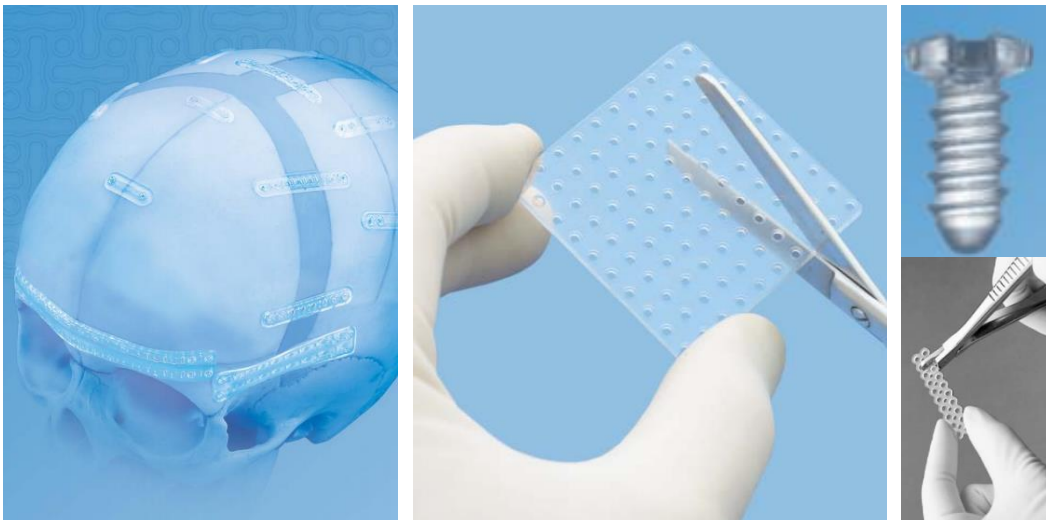

Figure 2 – Examples of resorbable bone screws and plates from Synthes PolyMax. Resorbable Fixation System.

1.2.5.2 PLA, PGA, and PLGA

PLA and PGA are composed of units of lactic acid and glycolic acid, respectively. Lactic acid has two active forms and can be present in its stereoisomers L- or D-configuration: poly-L-lactide (PLLA) or poly-DL-lactide (PDLLA). The physical

properties of the polymers depend on molecular weight, linear or branched structure, and amorphous or crystalline regions. Thus, different physical properties can be obtained by altering the components that make up the polymer structure. For example, a high molecular weight PLA may yield increased tensile and flexural strength but also increased time to complete degradation. An amorphous PLA will degrade in a shorter time frame because it is easier to decompose amorphous, unorganized regions over crystalline regions. [1, 2]

1.2.5.3 Degradation of resorbable systems

Degradation of PLA and PGA polymers happens in two stages *in vivo*. First, water hydrolyzes and attempts to depolymerize the material, which results in a reduction of molecular weight. Second, macrophages function to engulf and digest the low molecular weight "debris." This can be explained in three temporal events: 1) Reduction in molecular weight 2) Reduction in mechanical strength 3) Reduction in mass. Both PLA and PGA are initially degraded to lactic acid and glycolic acid respectively, metabolized by the liver, then excreted as carbon dioxide and water [1]. The speed of these events depends on many factors such as temperature, pH, availability of water, mechanical stresses, and the composition of the polymer itself such as molecular weight and crystallinity [2].

Because PLLA is a hydrophobic material, it can take close to five years to degrade fully *in vivo*. Some argue that a degradation time of such length causes PLLA to be considered clinically irrelevant from a resorbable standpoint. The

long term degradation also increases the risk of foreign body reactions [1]. On the other hand, PGA is a hydrophilic material, which welcomes the hydrolysis of water allowing for a much shorter degradation time. PGA loses its functional mechanical strength by 6 weeks and is completely degraded in less than six months [1, 16]. However, this shorter degradation time is associated with an inflammatory response, osteolysis, and sterile sinus formation due to the rapid degradation and accumulation of glycolic acid. Due to the rapid loss of structural properties and inflammatory reaction, PGA is rarely used alone as a fixation device [1].

The use of PLA or PGA materials individually can promote very long or fairly quick degradation rates but the combination of the two can provide an intermediate result [12]. Depending of the ratio of PGA:PLA, as shown in Table 1, the PLGA copolymer retains mechanical strength for 2 – 3 months and degrades in approximately 12 – 24 months which allows for a diminished inflammatory response and a clinically relevant fracture fixation device. The gradual degradation of the copolymer presents less risk of adverse side effects associated with the rapid degradation of PGA [1]. The ratios of PLA to PGA are manufacture specific but are often similar to 80:20 PLA:PGA.

While these resorbable polymers present obvious benefits as compared with metal bone screws, they also have *in vivo* complications. Due to the long degradation time of PLLA, there have been issues associated with long-term retention of the

screw. The screw may back out of the bone causing abrasion of any surrounding tissues. The portion of the screw that is threaded into the bone may degrade quicker than the screw head causing separation of the screw head. A loose screw head, floating freely in the body, could cause damage to surrounding tissues and inflammation [12].

Table 1 – Resorbable Rigid Fixation System Product Information Summary. [1]

	Stryker Inion CPS*	Synthes Rapid†	Biomet LactoSorb SE‡	KLS Martin Resorb X and SonicWeld Rx§
Composition	Varying combinations of L-polylactic acid; D,L-polylactic acid; polyglycolic acid; trimethylene carbonate	85:15 poly (L-lactide-*co*-glycolide)	82:18 poly L-lactic acid: polyglycolic acid	Both systems are 100% poly (D,L-lactic acid)
Degradation characteristics	BABY: strength retention 6–9 weeks; resorbed in 1–2 years ADULT: strength retention 9–14 weeks; resorbed 2–3 years	85% strength at 8 weeks; resorbed within 12 months	70% strength at 8 weeks, resorbed within 12 months	Strength retention to 10 weeks; resorbed in 1–2 years
Available sizes for craniomaxillofacial use	BABY system: 1.5 mm ADULT system: 1.5, 2.0, 2.5 mm 2.8/3.1-mm (screws only)	1.5-mm system 2.0-mm system	1.5-mm system 2.0-mm system 2.5/2.8-mm (screws only)	Both Resorb X (screws) and SonicWeld Rx (pins): 1.6-mm system; 2.1-mm system
Plate profile (thickness)	1.5-mm system: 1.0 mm 2.0-mm system: 1.3 mm 2.5-mm system: 1.7 mm	1.5-mm system: 0.8 mm 2.0-mm system: 1.2 mm	1.5-mm system: 1.0 mm 2.0-mm system: 1.4 mm	Resorb X and SonicWeld Rx: all plates shapes 1.0 mm
Screw placement	Self-drilling tap or separate tap	Self-drilling tap or separate tap	Self-drilling tap or separate tap; push screws (no tapping required)	Resorb X: screws with self-drilling tap SonicWeld Rx: drill hole for pins and secure with ultrasonic frequency welder (no tapping required)
Indicated for mandible fractures	Yes (with IMF only)	No	No	No

*Inion CPS Biodegradeable Fixation System [product guide]. Kalamazoo, MI: Stryker Craniomaxillofacial; 2008.
†Rapid Resorbable Fixation System [product guide]. West Chester, PA: Synthes CMF; 2008.
‡Lorenz Plating System LactoSorb [product guide]. Jacksonville, FL: Biomet Microfixation; 2008. Note: Biomet was formerly known as Walter Lorenz Surgical (Jacksonville, FL).
§SonicWeld Rx [product guide]. Jacksonville, FL: KLS Martin – LP; 2008.

1.2.5.4 Discussion on clinical use

While the mechanical properties of resorbable devices are much weaker than metallic components, the complications are less influenced by fracture fixation but by the handling and installation of the resorbable plates and screws. The

implantation technique from the surgeon's point of view is not ideal. The fragility and poor torsional properties of resorbable screws emphasizes careful pre-tapping of the screw hole and insertion while the plates need to be pre-shaped to the exact curvature of the fracture location [1, 2, 17]. Plates and screws need to be larger than their metal counterparts due to the lower strength and stiffness and, thus, there may be increased palpability in thin skin cover areas, at least initially, for the patient [1]. Flexure of the resorbable plates is only possible above the glass transition temperature of the polymer (approximately 60ºC) so plates need to be preheated prior to shaping. Devices such as heating pads and probes or heated baths are possible for plate shaping. However, uncontrolled heating of the plates may affect the molecular structure of the polymer effecting stability, strength, and degradation properties [2]. Uncontrolled heating may result as a consequence of inexperienced plate shaping where the plate needs to be reheated and shaped multiple times to properly conform to the bone interface. While metal devices can be resterilized for up to 50 cycles in an autoclave, resorbable systems cannot, thus, limiting their usable lifetime and also creating increased costs. Due to these complications and incomplete material profiles of resorbable screws and plates, metal devices still remain the gold standard for fracture fixation.

Despite the complications with implantation, these devices may result in improved bone remodeling after injury by allowing earlier functional exposure of the fracture gap to stresses which allows faster remodeling of the injury; micromotion at the fracture site allowed by resorbable implants may accelerate

healing compared to rigid fixation with metallic devices [1, 2]. These potential benefits have supported the clinical use of bioabsorbable screws and plates for the internal fixation of fractures [1, 8, 9, 17-22]. However, resorbable materials now on the market are associated with inflammatory reactions, can generate sterile sinus formation, result in incomplete remodeling of the bone, and improper dynamics between device strength retention and wound healing and in some cases, have induced osteolysis [1, 7, 16, 18, 20, 23]. Nevertheless, the complication rate of resorbable systems is estimated to be 6% which compares favorably to metal hardware removal rate of 10% [1]. Figure 3 shows an example of incomplete remodeling of the bone. It depicts the fractional cross-sectional occurrences of natural tissue elements found in bone. A comparison was made between an intact bone as a control, an empty hole, and holes filled with PGA and PLLA screws. The graph shows that neither resorbable device was capable of regenerating boney tissue elements in a similar fashion to an intact bone or even an empty hole after a 54 month time point.

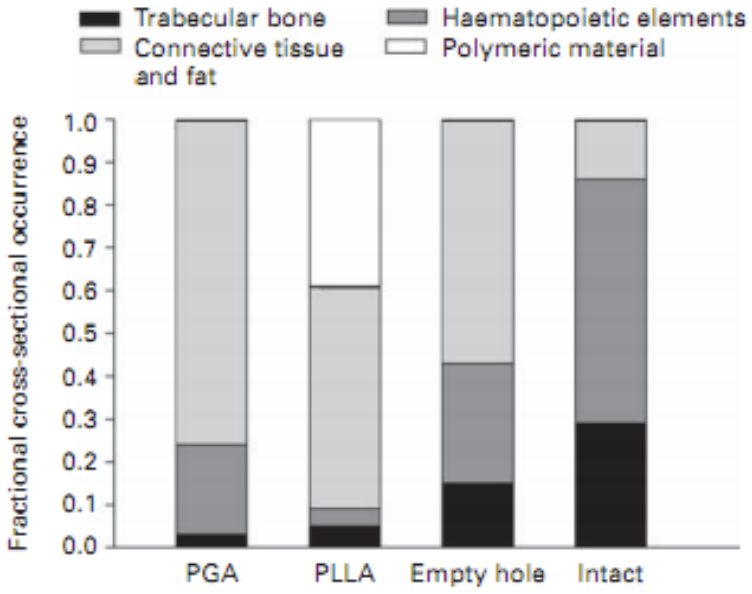

Figure 3 – Bar chart showing the occurrence of the natural boney tissue elements and polymeric material in the 54-month specimens (PGA, polyglycolic acid; PLLA, poly-laevo-lactic acid). [16]

1.2.6 Criteria for choosing metal versus resorbable fracture fixation systems

The ideal material provides sufficient strength of fixation to maintain fracture reduction and resists physiologic stresses until fracture healing is complete while also being malleable to allow for plate shaping *in situ* [1]. The plates should be thin enough to minimize problems with visibility, palpability, thermal sensitivity, and discomfort, yet still maintaining sufficient strength to sustain fracture reduction. Other important characteristics include shear strength to maintain the stability of the screw head, limited foreign body response, and proper bone remodeling and ingrowth. As shown in Table 2, when deciding between a metal and resorbable system, patient specific conditions such as age, location of the fracture and severity, load-bearing versus non-load bearing applications, hardware costs, and comparative complication rates all influence the decision [1]. For

example, an adult patient with an orbital fracture, with limited load bearing needs, can receive a metallic or resorbable device but may have a lower incidence of adverse side effects with the resorbable device if installed properly. A patient with multiple fractures in the CMF complex may receive all metallic implants simply due to the time, ease, and minimal errors associated with implantation of metallic hardware. Pediatric patients should almost always receive resorbable hardware in order to avoid potential complications with growth restriction; metallic hardware removal in pediatric patients is not conditional, but required [1]. Cost is a factor in all these cases as resorbable plates are 20% more expensive than metallic plates where screws are virtually the same price. For a fracture fixation device system consisting of 2 L-plates, 1 orbit rim plate, 1 orbit floor implant, 16 screws, and 1 disposable drill bit/tap, the resorbable system costs $2433.00 versus $2381.00 for the titanium system. However, the titanium systems have an additional cost benefit due to the ability to be resterilized [1]. In all likelihood, metallic and resorbable fixation systems will always coexist with each being used for specific applications.

Table 2 – Comparison of metallic and resorbable fracture fixation systems.

Type	Pros	Cons	Complication Rates	Application

Metallic	• Ease of implantation
	  • Self-tapping screws
	  • *In situ* plate shaping
	• Robust mechanical properties
	• Resterilization/reuse
		• Stress shielding
		• Temperature sensitivity
		• Plate exposure or migration
		• Corrosion
		• Growth disturbance in children
		• Palpability
		• Limited radiological imaging
		• Infection
			~ 10%	• All except pediatric craniofacial
				• Load bearing applications

Resorbable	• Improved bone remodeling and accelerated healing
	• Degradable device
	• Flexibility for growing bones
		• Laborious implantation technique
		  • Pre-drilling and tapping of hole
		  • Heat to shape plates
		• Degradation to acidic products
		• No resterilization/reuse
		• Inflammatory reaction
		• Sterile sinus formation
		• Osteolysis
			~ 6%	• Pediatric craniofacial
				• Non-load bearing applications

1.2.7 Silk Background

1.2.7.1 Overview

Silk has been utilized in many biomedical applications in various different formats. Physicians have used silk for centuries as a suture material but it has recently gained attention for other applications, as shown in Table 3 and Figure 4, such as native fibers for ACL regeneration, regenerated fibers, electrospun fibers, sponges, gels, films, and microspheres [24]. Silk fibroin protein can be decomposed and extracted from silk cocoons then recapitulated into various different structures.

Table 3 – Current applications, tissue types, and material formats of silk. [24] HFIP (1,1,1,3,3,3 Hexafluoro-2-propanol)

Application	Tissue type	Material format
Tissue engineering		
	Bone	HFIP sponges
		Aqueous sponges
		Electrospun fibers
	Cartilage	HFIP sponges
		Aqueous sponges
		Electrospun fibers
	Soft tissue	HFIP sponges
		Aqueous sponges
		Hydrogels
	Corneal	Patterned silk films
	Vascular tissues	Tubes
		Electrospun fibers
	Cervical tissue	Aqueous sponges
	Skin	Electrospun fibers
Disease models		
	Breast cancer	HFIP sponges
		Aqueous sponges
	Autosomal dominant polycystic kidney disease	Aqueous sponges
Implant devices		
	Anterior cruciate ligament	Fibers
	Femur defects	HFIP sponges
	Mandibular defects	Aqueous sponges
Drug delivery		
	Drug delivery	Spheres
	Growth factor delivery	Spheres
	Small molecule	Spheres

Note: The sources for the reagents and equipment described in these protocols are given only as examples. Equivalent materials can be used unless otherwise noted.

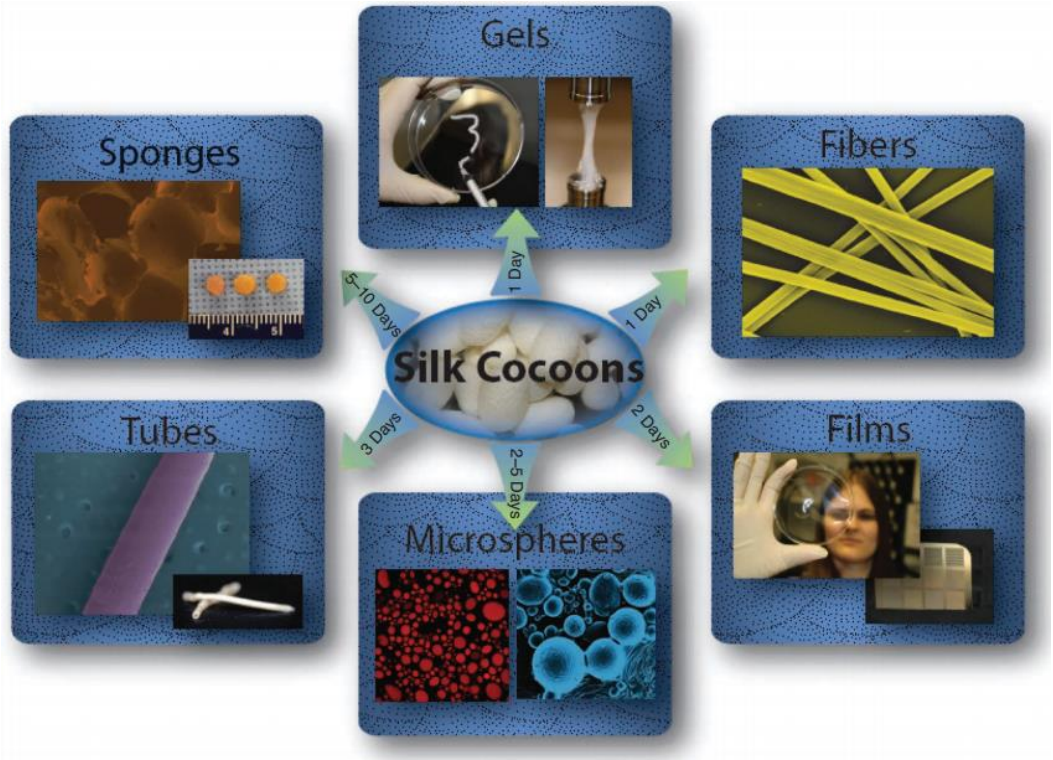

Figure 4 – Schematic of material forms fabricated from silk fibroin using both organic solvents and aqueous-based processing techniques. [24]

Silk is used in medical applications due to its robust mechanical properties (high tensile strength and large extensibility), biocompatibility, and tunable degradation [24, 25]. Silk was chosen as the material to optimize because of numerous beneficial and tunable properties. Similar to polyesters, the composition of silk can be altered to affect the mechanical and degradation profiles. However, silk degrades to non-inflammatory products of amino acids. Silk degrades by surface erosion allowing for a more predictable degradation because the implant will gradually lose strength as it diminishes in size. Polyesters, such as PLA or PGA, degrade by hydrolysis so they may break down from within resulting in a catastrophic failure at a certain time point.

1.2.7.2 Multifunctional benefits of silk

Silk is biocompatible and FDA-approved for some applications (Allergan Medical) and has been utilized due to its myriad of functional properties. Silk is degradable *in vivo* with controllable rates from days to years [26] and can provide robust mechanical properties when reinforced with microfibers [27]. Along with these beneficial properties for tissue engineering, a strong yet degradable biomaterial, silk can also be functionalized for the delivery of bioactive compounds such as bone morphogenic protein (BMP) or antibiotics such as vancomycin; silk can be loaded or coated with the bioactive compounds to stabilize and deliver once implanted *in vivo* [28-34]. Silk is also stable to > 170ºC reducing temperature sensitivity of the implant and allowing for easy autoclave sterilization [35, 36]. Many patient problems require post-operative imaging; silk is invisible to x-rays and allows MRI imaging. While the current gold standard for osseous-fixation devices is metal and, thus, limits MRI imaging, silk provides an alternative that allows MRI imaging in the case of a soft tissue injury in combination with a bone fracture.

1.2.7.3 Secondary structure of silk

Silk cocoons can be decomposed into silk fibroin solutions which are the basis for many of the applications listed above. Silk fibroin is typically composed of three distinct secondary structures: random coil (Silk I), α-helix, and β-sheet (Silk II) [37, 38]. The secondary structure of silk is closely related to its function so secondary structures are very important in determining physical properties and

function of the silk [39]. Silk I is obtained when silk solutions or dope from the silkworm gland is allowed to dry without mechanical disturbance. Silk I is an unorganized structure with no real alignment that does not yield great mechanical properties. Silk in the α-helix phase is a metastable phase composed of α-helices that can be transitioned to Silk I with heat or Silk II with mechanical stresses or methanol. Silk II has a crystalline composition of anti-parallel β-sheets that are preferably aligned along the silk fiber axis to maximize strength. When processing silk fibroin into mechanically strong constructs, the goal is to stabilize the secondary structure with the highest crystalline alignment parallel to the direction of the primary stresses.

1.2.8 1,1,1,3,3,3 Hexafluoro-2-propanol interaction with peptides

1.2.8.1 Overview

1,1,1,3,3,3 Hexafluoro-2-propanol (HFIP), and other fluorinated solvents such as trifluoroethanol (TFE), have been characterized as one of the most effective methods of stabilizing α-helical structures in peptides [40]. Alcohols denature the native state of proteins and can stabilize the α-helical conformation in unfolded proteins and peptides. Proteins such as bovine β-lactoglobulin have been shown to transform from their native state, β-sheet confirmation, to the α-helical state whereas melittin transformed from the unfolded state to the α-helical state [41]. Because of the increased ability of fluorinated solvents, such as HFIP and TFE, to induce α-helical structure, it is reasoned that the fluorine (F) atom is important in enhancing the effect of the alcohol. HFIP has six (hexa) F atoms where TFE has 4

(tetra) F atoms indicating that HFIP may be more effective in α-helical stabilization than TFE. In both β-lactoglobulin and melittin, HFIP exhibited the highest effectiveness of inducing α-helical structures over other structures with the order being: HFIP > TFE > isopropanol > ethanol > methanol [41]. The change in free energy ΔG_H of the transition to the helical state decreased linearly with an increase in alcohol concentration. HFIP required the lowest alcohol concentration to cause ΔG_H to be negative indicating that the change to an α-helical state is more spontaneous for peptides dissolved in HFIP than other alcohols.

1.2.8.2 HFIP interaction with silk

Because of the ability of HFIP to stabilize α-helical structures in peptides and its established work with silk, HFIP silk solutions were used as the basis for the new silk fracture fixation device. Previous work with regenerated silk fibers shows the ability of HFIP to stabilize an ordered, helical structure, in HFIP silk solutions. These solutions can be convert to a crystalline β-sheet format when treated with methanol [42]. The artificial spinning process of HFIP silk fibers produces high strength fibers. Groups have shown the ability to make high strength regenerated silk fibers that can degrade using HFIP silk solutions [43]. Further, HFIP allows for a high packing density of silk in solution, thus, allowing for more silk to be packed in the same volume; an increased density of silk will allow for better mechanical properties. Because resorbable devices require high strength but also

degradation in a prescribed time frame, HFIP silk solutions were used as the basis for this research.

1.2.9 Bone

1.2.9.1 Overview of structure

There are various different levels of the hierarchical structural organization of bone as shown in Figure 5. First, the macrostructure consists of cancellous and cortical bone. Cortical bone, or compact bone, forms the outer shell of most bones while cancellous bone, or trabecular bone, is less dense and more spongy and is typically found at the end of long bones. Cortical and cancellous bone can easily be distinguished by their porosity or density. Second, the microstructure (10 – 500 μm) is composed of Haversian systems, osteons, and single trabeculae. Third, the sub-microstructure (1 – 10 μm) is made up of lamellae. Lamellae are sheets of mineralized collagen that can be wrapped in concentric layers around a central canal to form an osteon or Haversian system. Fourth, the nanostructure (100s nm – 1 μm) consists of fibrillar collagen and embedded minerals. Finally, the sub-nanostructure (≤ 100s nm) is composed of the molecular structure of all of the constituent elements such as minerals, collagen, and non-collagenous organic proteins. [44]

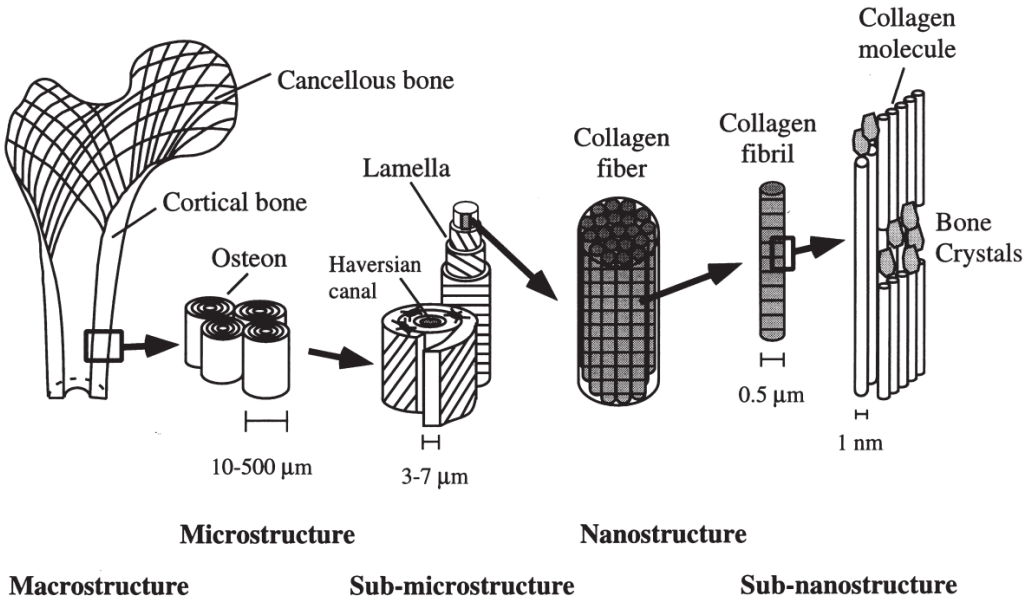

Figure 5 – Hierarchical structural organization of bone: (A) Cortical and cancellous bone. (B) Osteons with Haversian systems. (C) Lamellae. (D) Collagen fiber assemblies of collagen fibrils. (E) Bone mineral crystals, collagen molecules, and non-collagenous proteins. [44]

The hierarchical structure of bone allows for a diverse set of mechanical, biological, and chemical functions including structural support, protection, and storage of healing cells [44]. However, the structure of bone that drives mechanical and structural function often differs at different structural levels, between different bones [44], at different levels of mineralization, as well as between different people based on age, sex, and physical condition [45].

1.2.9.2 Remodeling process of bone

Bone remodeling is a biphasic process where old or damaged bone is resorbed by osteoclasts and new bone is formed by osteoblasts (ossification) [46]. Osteoclasts break down old or damaged bone so that osteoblasts can deposit new bone to ensure a mechanically sound structure. A disproportionate ratio of resorption to

formation can result in metabolic bone diseases such as osteoporosis which reduces the density of bone. Remodeling will also respond to mechanical stimuli. In a damaged bone, inflammatory cells such as macrophages, vascular cells, osteochondral progenitors, and osteoclasts are key cellular members in the repair and remodeling process which can be affected by pro-inflammatory cytokines and growth factors, pro-osteogenic factors, and angiogenic factors [47]. Osteoclasts are from the same lineage as macrophages but are distinct in that they are involved in bone remodeling.

1.2.9.3 Microhardness of bone

Hardness is defined as the resistance of a material to being penetrated by an indenter and hardness measurements can be used to assess the resistance of a material to deformation [45, 48]. A hardness test consists of extending an indenter into a material with a set, applied load until an impression is made. Based on the specific test method and parameters, the impression can be measured and converted into a hardness value. There are both macrohardness and microhardness tests but microhardness tests are typically used for lower applied loads and good for testing softer materials. The two main microhardness tests are the Knoop (HK) and Vickers (HV) microhardness tests. The Knoop test uses a diamond indenter that is pyramidal in shape with a length to width ratio of 7:1. The Vickers test also used a diamond indenter that is pyramidal in shape but with a length to width ratio of 1:1. Both indenters are made of diamond because diamond is one of the hardest materials and will not be indented by the material being tested.

Vickers microhardness is a common method for testing the hardness of bone in literature. There are a wide range of values reported for the microhardness of bone but many investigators report microhardness numbers typically in the range of 40 – 60 kg/mm^2 [45, 49, 50]. Table 4 and Figure 6 show the variation in Vickers microhardness measurements of bone for human control and osteoporotic patients. Clearly, there is a wide range of microhardness values reported but most values seem to fall within the 40 – 60 kg/mm^2 range.

Table 4 – Variation of Vickers microhardness measurements of bone for human control and osteoporotic (OP) patients. [45]

Human subjects	Total bone		
	Hv_{25} (kg/mm^2)	DMB (g/cm^3)	HI (g/cm^3)
19 Controls	49.18 ± 1.82	1.10 ± 0.09	0.22 ± 0.07
52 OP patients	44.10 ± 4.72*	1.03 ± 0.07*	0.25 ± 0.07
30 OP men	40.52 ± 1.88#	1.02 ± 0.06#	0.23 ± 0.06
22 OP women	48.97 ± 2.46	1.05 ± 0.08	0.28 ± 0.07
13 control men	48.96 ± 1.85	1.10 ± 0.09	0.22 ± 0.08
6 control women	49.71 ± 2.01	1.10 ± 0.08	0.21 ± 0.03

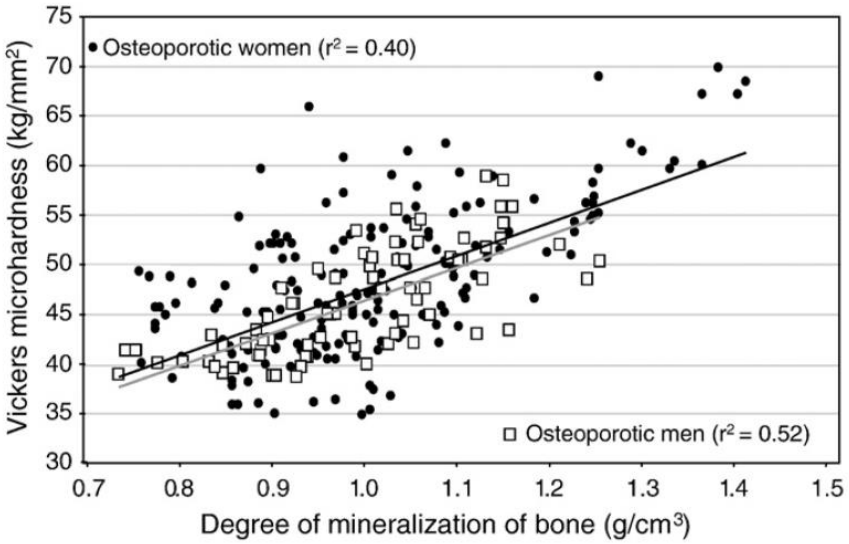

Figure 6 – Variation in bone hardness measurements between different patients. [45]

Many investigators report the differences in microhardness values of bone based on age, sex, degree of mineralization of bone (DMB), mass, size, density, geometry, and microarchitecture. For example, in various bones, microhardness, Young's modulus, and mineral content increase with age. [45, 50]

2. Objective

Metallic systems will always be used for load bearing applications and when speed/ease of implantation is crucial for a successful outcome. Thus, the goal of the new fracture fixation device is to surpass current resorbable devices. Current resorbable devices are not widely accepted due to their laborious implantation technique for both screws and plates and limited application areas. Many resorbable devices are simply wasted because they cannot be resterilized or reused once opened in the operating room. The specific goals of a new fracture device are biodegradability in 12 months or less, an implantation technique similar to metallic devices (self-tapping screws and straightforward plate shaping), ability to be resterilized for reuse, and better mechanical properties than current resorbable devices in order to be applied to more application areas.

3. Experimental Methods

3.1 Preparation of silk solutions

3.1.1 Preparation of vacuum dried silk for 30 minute boil

Silk was prepared using established purification protocols as shown in Figure 7 [24]. Taiwanese *Bombyx mori (B. mori)* cocoons were boiled for 30 minutes in aqueous 0.02 M Na_2CO_3, and then rinsed for 3 x 30 minutes in distilled water to remove the Na_2CO_3 and sericin. The degummed cocoons were allowed to dry for more than 12 hours and then subsequently dissolved in 9.3 M LiBr solution at 60ºC for 3-4 hours. The solution was dialyzed for 2 days in distilled water using Slide-a-Lyzer dialysis cassettes (MWCO 3,500) from Pierce Protein and Biology Products (Rockford, IL, USA). The solution was centrifuged in a Sorvall RC-5B Refrigerated Superspeed Centrifuge (Dupont Instruments, Wilmington, DE, USA) at 18,000 RPM for 2 cycles of 20 minutes each. The concentration was determined by measuring a volume of solution and the final dried weight. The final solution, 6 to 8 weight(g)/volume(ml)%, was frozen for 2-5 days and freeze dried at -20 or 0°C until complete sublimation (transition of a substance from the solid phase to gas phase without passing through the liquid phase). The freeze dried silk was stored in ambient conditions covered with tin foil to prevent any rehydration of the lyophilized solution until used in the processing steps below. The 30 minute boil solutions were used for all tests.

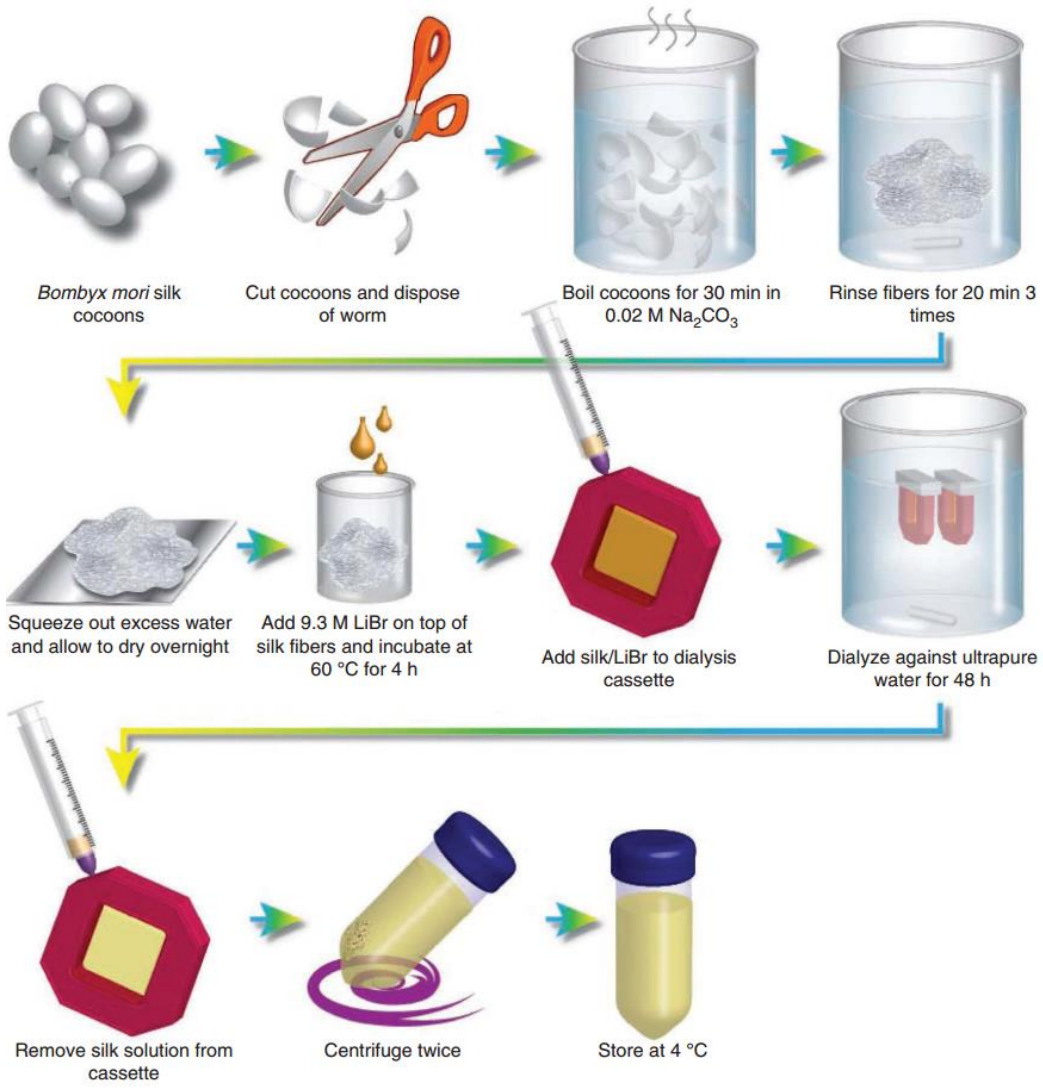

Figure 7 – Schematic of the silk fibroin extraction procedure. Going from the raw material (cocoons) to the final aqueous-based solution takes 4 days.

3.1.2 Preparation of 1,1,1,3,3,3 Hexafluoro-2-propanol (HFIP) silk solutions

The vacuum dried silk was resolubilized in 1,1,1,3,3,3 hexafluoro-2-propanol (HFIP) (puriss., ≥ 99.0% (GC)) from Sigma-Aldrich (St. Louis, MO, USA) to generate solutions for preparation of the devices. Figure 10 illustrates the entire silk screw and plate fabrication process from aqueous silk solution to the final geometries of the screws and plates. Before dissolving in HFIP, the vacuum dried

silk was processed in a Waring blender (Stamford, CT, USA) so that the pieces could be tightly packed into a syringe. For 25 w/v% silk in HFIP, 3 g of vacuum dried silk was added to 30 ml syringes and then 9 ml of HFIP was added. The solubilized HFIP silk solutions were stored at ambient temperatures until used in the molding steps below.

3.2 Preparation of HFIP silk screw and plate blanks for machining

Silk screw blank molds, as shown in Figure 8, were prepared using wax from MachinableWax.com (Traverse City, MI, USA) and machined to 1.3 in (3.30 cm) height with 6 through holes of 0.30 in (0.76 cm) diameter. A thin wafer of 0.10 in (0.25 cm) was also machined to act as a base for the mold. The thin wafer was attached to the base of the mold by melting both edges of the wax and then allowing it to dry. Silk plate blank molds (Figure 8) were prepared using wax that was machined into a rectangular mold with inner dimensions of 1.75 x 1.75 x 1.3 in^3 (4.45 x 4.45 x 3.30 cm^3). Once the screw and plate molds were filled with HFIP silk solutions, they were placed into 100% methanol (Certified ACS Reagent Grade) from Thermo Fischer Scientific Inc. (Pittsburg, PA, USA) for 3 – 4 days to induce the beta sheet conversion and also to displace the HFIP. Subsequently, a methanol to water gradient was used and deionized water was added 4 times at 1 hour intervals to slowly transition the solution from 100% methanol and HFIP to 100% water. Post gradient water changes were used to remove residual HFIP. The materials were then dried in a fume hood or 60°C oven for at least one week and then autoclaved before machining.

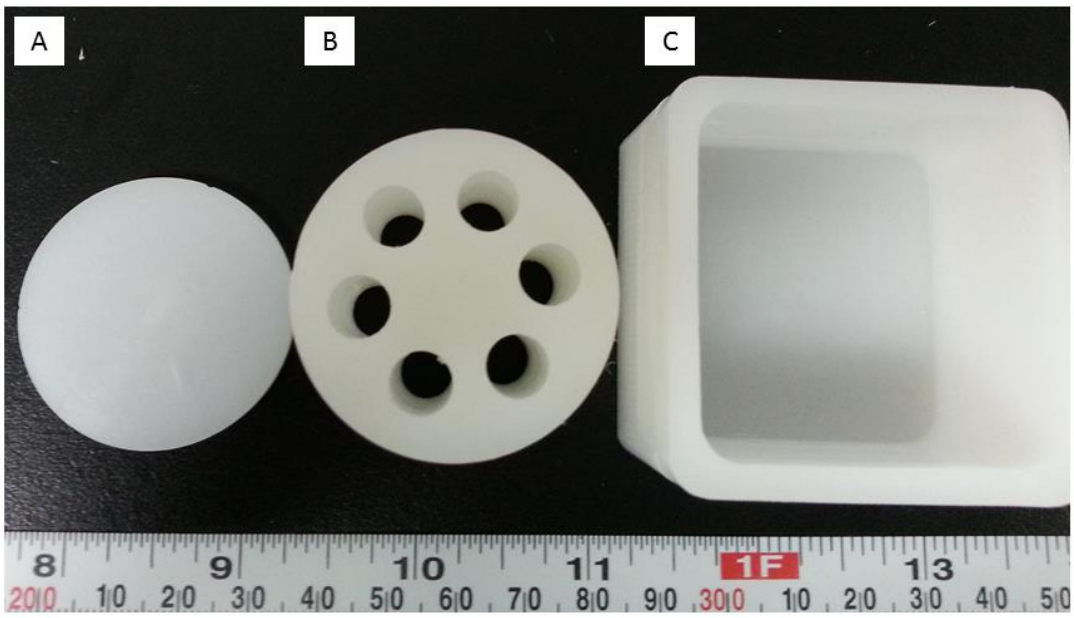

Figure 8 – Machinable wax molds for screw and plate blanks. (A) Thin wafer that acts as a base for the screw blank mold; 1.0 in (2.54 cm) diameter and 0.10 in (0.25 cm) thickness (B) Screw blank mold; 1.3 in (3.30 cm) height with 6 through holes of 0.30 in (0.76 cm) diameter. (C) Plate blank mold; 1.75 x 1.75 x 1.3 in^3 (4.45 x 4.45 x 3.30 cm^3).

3.3 Machining of silk screws and plates

The silk blanks were machined using a MicroLux True-Inch 7x16 Variable Speed Lathe (Micromark, Berkeley Heights, NJ, USA) as shown in Figure 9. For the screws, the blanks were cut to the outside diameter and head diameter of the desired screw size. While the screw remained attached to the blank on the lathe, a 1-72 NF Die 13/16 OD (McMaster-Carr, Robbinsville, NJ, USA) was used to machine the threads into the screw shank. The screw was cut off behind the head. A diamond cutter was mounted to the lathe and a slot was cut in the screw heads. For the plates, a diamond cutter, sand paper, and milling machine were used to reduce the oversized blank into desirable plate thicknesses and a razor blade was used to cut the plates into various geometries.

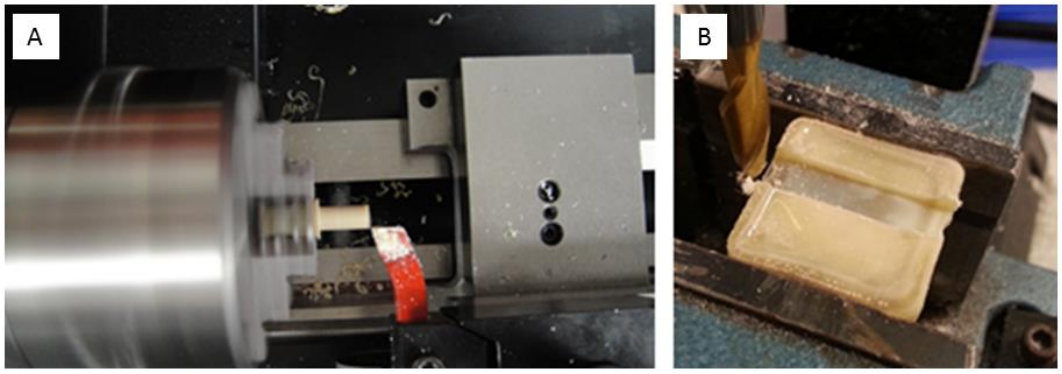

Figure 9 – Machining of silk material using a lathe (A) and mill (B).

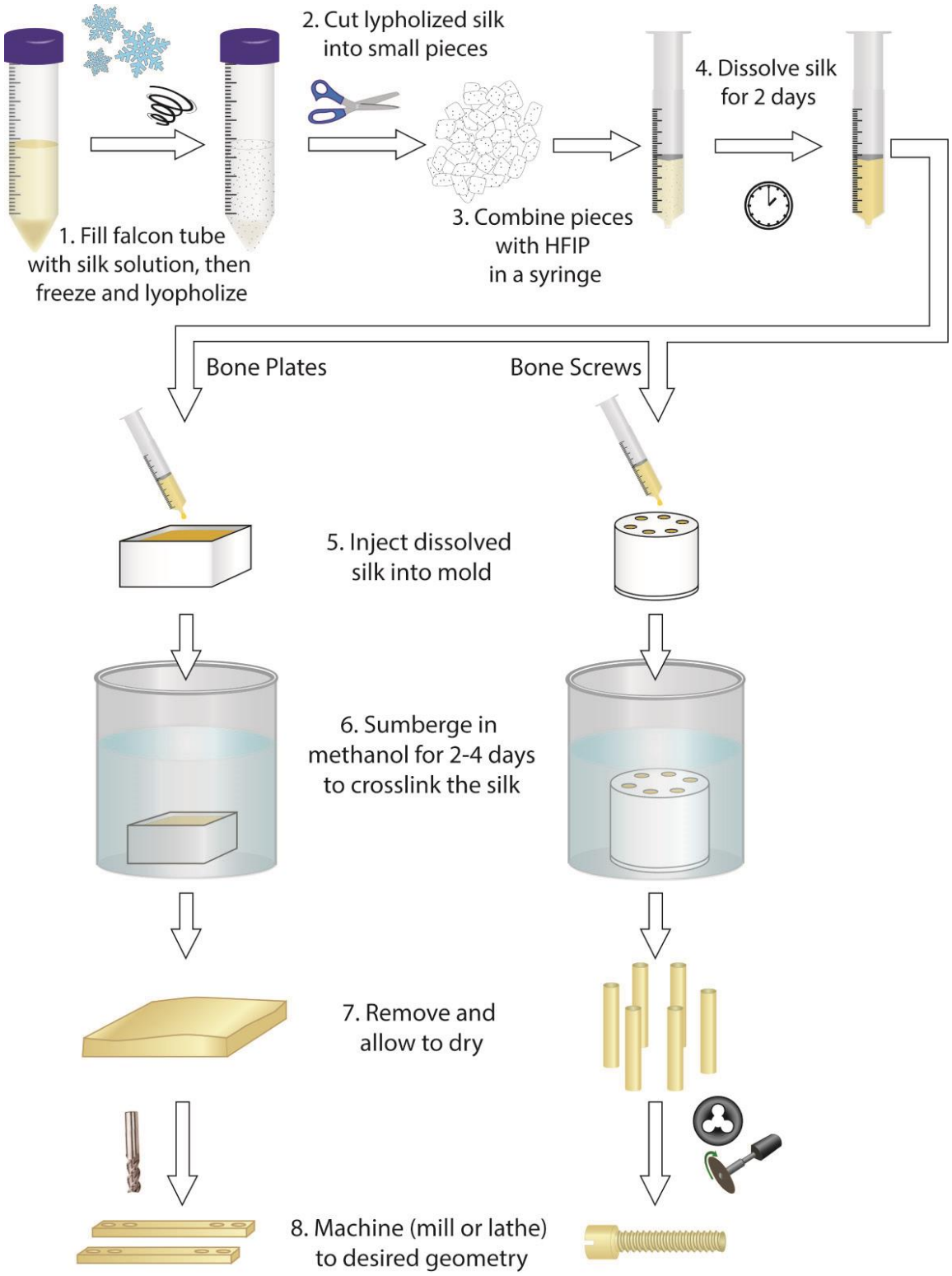

Figure 10 – Bone screw and plate processing diagram from aqueous silk solution to final screw and plate geometries.

3.4 Structural and morphological Analysis

Conformation of the silk material was analyzed with a JASCO FTIR 6200 spectrometer (Jasco Analytical Instruments, Easton, MD, USA) using a MIRacle attenuated total reflection (ATR) accessory with Ge crystal (Pike Technologies, Madison, WI, USA) and analysis was performed as previously described [51]. Fourier self-deconvolution of the amide I region was performed using OPUS 5.0 software (Bruker Optics, Billerica, MA, USA) with a half-bandwidth of 27 cm^{-1} and a noise reduction factor of 0.3. For surface morphological analysis, samples were sputter coated with a SC7620 Sputter Coater from Emitech (Fall River, MA, USA) for 90 – 120 seconds and then imaged using a ZEISS EVO MA10 scanning electron microscope (SEM) (Oberkochen, Germany).

3.5 Mechanical properties

3.5.1 Double lap shear

The double lap shear test consisted of three adjacent stainless steel plates with an aligned 1.5 mm hole (Figure 11A). The 1.5 mm silk pins were machined to fit snugly through the fixture. The fixture was mounted onto an Instron 3366 (Norwood, MA, USA) test frame. The bottom fixture remained stationary while the top fixture was compressed at a rate of 5.0 mm/min until fracture of the silk pin (ASTM standard F2502-11: Standard Specification and Test Methods for Absorbable Plates and Screws for Internal Fixation Implants, [52]). The maximum stress (MPa) was reported. Tests were performed in dry and hydrated environments, by immersion in Dulbecco's Phosphate Buffered Saline (PBS)

solution (Invitrogen, Grand Island, NY, USA) at 37°C for 24 hours. The tests were then performed in a 37°C bath of PBS.

3.5.2 Pull-out strength

Pull-out strength consisted of an artificial bone block in accordance with ASTM standard F1839-08 (Standard Specification for Rigid Polyurethane Foam for Use as a Standard Material for Testing Orthopaedic Devices and Instruments) to fix the threads and a stainless steel screw head holder. The artificial bone block was drilled with a #53 drill bit (1.5 mm diameter) but was not tapped. As shown in Figure 11B and C, the 1-72 machine style silk screws were generated and then placed in the head holder and then screwed into the artificial bone block. The head holder was then fastened to an Instron 3366 test frame and extended in the tensile direction at a rate of 5.1 mm/min (ASTM standard F2502-11, [52]). Tests were performed in dry and hydrated environments, by immersion in PBS solution at 37°C for 24 hours. The tests were then performed in a 37°C bath of PBS.

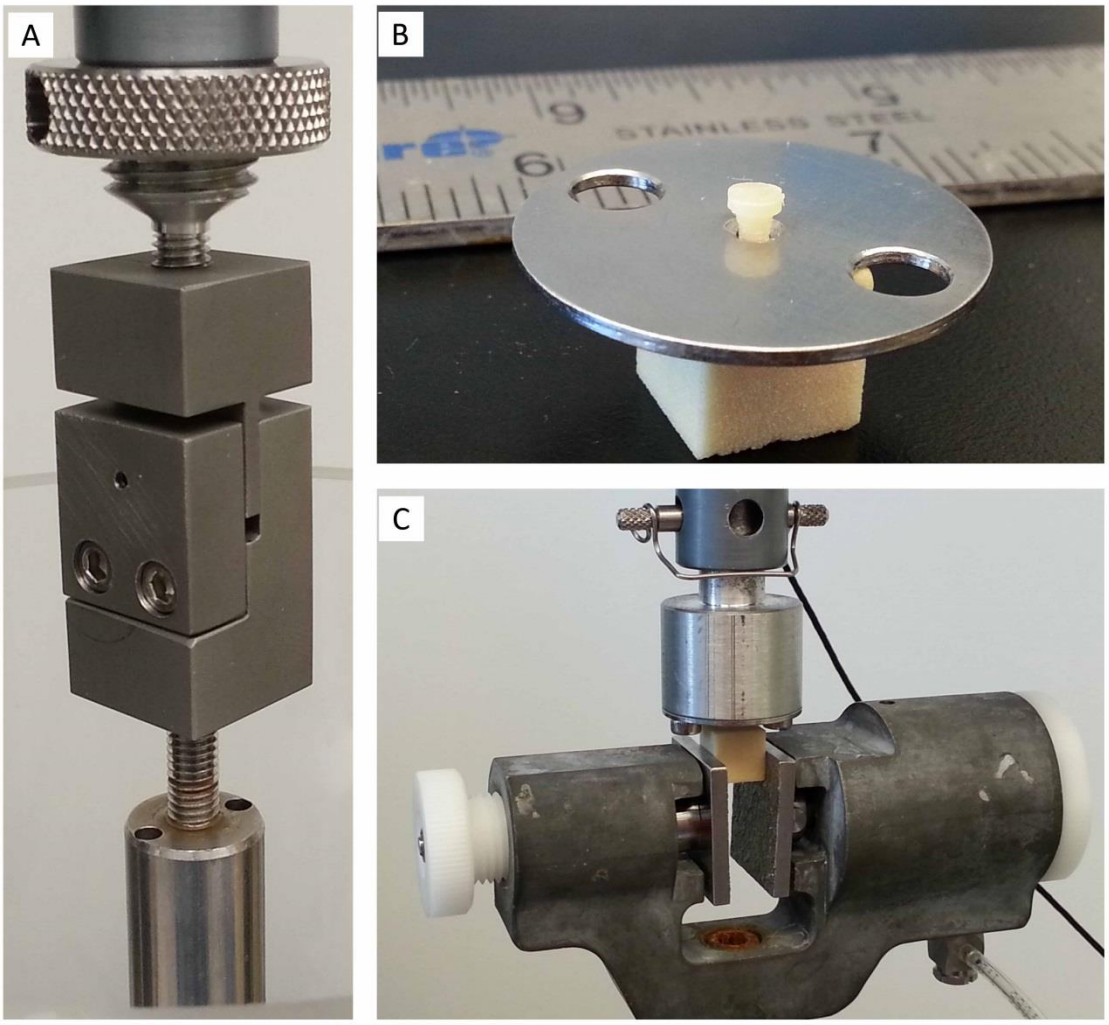

Figure 11 – Mechanical testing fixtures. (A) Double lap shear fixture with 1.5 mm hole. (B) Silk screw fixed in head plate and artificial bone. (C) Dry pull-out test of silk screw.

3.6 *In vitro* enzymatic degradation

The degradation of the silk screws was studied using Protease XIV (Sigma-Aldrich, St. Louis, MO, USA) with an activity of 5 U/ml following previously published procedures [53, 54]. Silk plugs (0.00023 oz. (0.0065 g), 0.059 in (1.50 mm) major diameter, 0.118 in (3.00 mm) overall length) were placed in well plates with 2 ml of PBS (pH 7.4) containing enzyme and PBS alone for control at 37°C. The enzyme solution was replaced every 24 – 48 hours with freshly

prepared solution. Samples were sacrificed at 1, 4, 8, and 23 weeks and dried, weighed, and imaged using an SEM to determine degradation.

3.7 Swelling properties

The silk screws were machined and then immersed in distilled water for 24 hours. Surface moisture was removed from the sample by wiping with a Kimwipe (Kimberly-Clark, Dallas, TX, USA) and the wet weight of the sample taken (Ws). The samples were dried, and then the dry weight of the sample was taken (Wd). The swelling ratio and water uptake (%) were calculated.

$$\text{Equation 1 – Swelling ratio} = (Ws - Wd) / Wd$$
$$\text{Equation 2 – Water uptake (\%)} = [(Ws - Wd)/Ws] \times 100$$

3.8 Vickers microhardness

Cylindrical silk blanks were mounted in an epoxy mounting kit from Buehler (Lake Bluff, IL, USA) as shown in Figure 12. EpoKwick Epoxy Resin (Part number: 20-8128-032) was mixed with EpoKwick Epoxy Hardener (Part number: 20-8128-008) in a ratio of 5:1 resin to hardener. SamplKups 1 in (Part number: 209178) were first coated in Release Agent (Part number: 20-8185-002) then the silk sample face that was tested for hardness was placed face down in SamplKups. The resin, hardener mixture was poured over the top just enough to cover the sample. The samples were allowed to set for 24 hours, and then removed from the SamplKups. A Low Speed Buehler Polisher was used with 8 inch sanding disks to expose the surface and to get a smooth, flat surface for hardness testing. Sanding was performed with increasing grit sandpaper (120, 240, 320, 400, then 600 grit).

Finally, a paper towel was dipped in 100% methanol and used to clean the sanded surface. No polishing agents were used during the sanding of the material due to potential effects on the material properties.

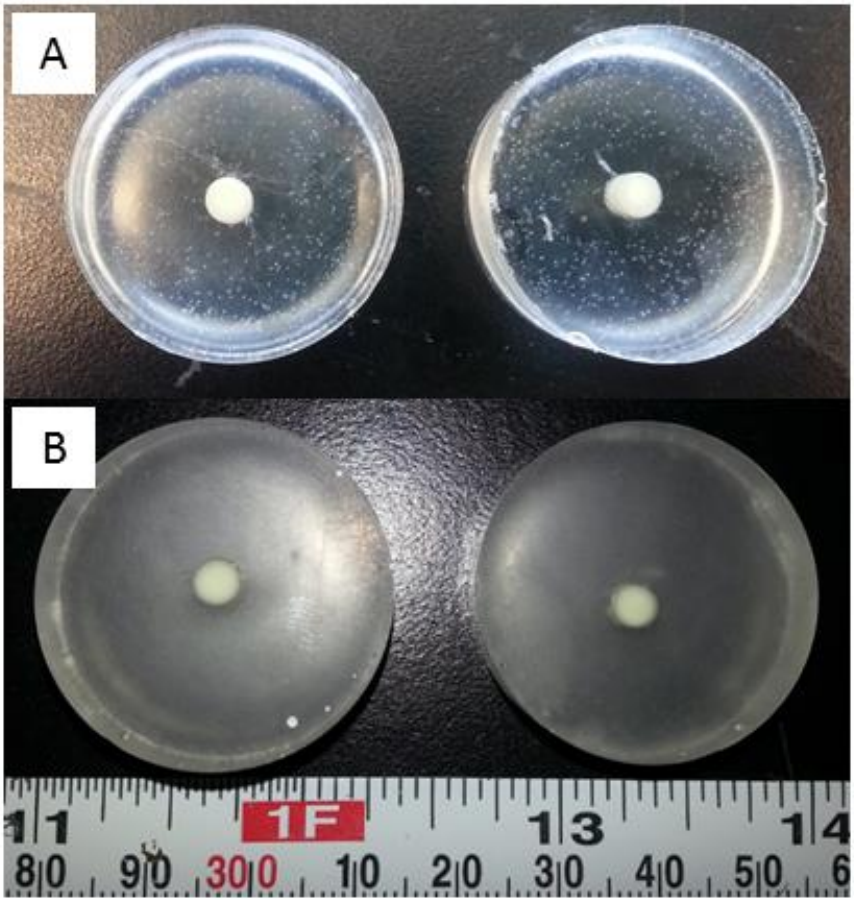

Figure 12 – Mounting of silk samples in epoxy. (A) Silk sample in hardened epoxy prior to sanding. (B) Exposed, smooth silk sample prior to hardness testing.

Once smooth and flat, the samples were tested on a Tukon 2100 Microindentation/Vickers Hardness Tester from Instron (Norwood, MA, USA) as depicted in Figure 13. A Vickers diamond indenter with a 300 gram force load (Hv 0.3) was applied over a 3 second period then allowed to dwell for 10 seconds. This protocol was altered from similar protocol performed on other biomaterials and bone [48-50, 55, 56]. The microscope on the indenter was used at 20X power

in combination with the Wilson-Wolpert Measurement System (Figure 14) to view the indent. The "Measure this indent manually" tool was used to determine the length of the diagonals and the resulting Vickers hardness number. For manual calculation, Equation 3 can be utilized.

Equation 3 – $Hv = 1854.4P/d^2$ (where P is the load in grams, d is the average of the two diagonals in microns, and Hv is in kg/mm^2) can be used to calculate the Vickers microhardness value [45].

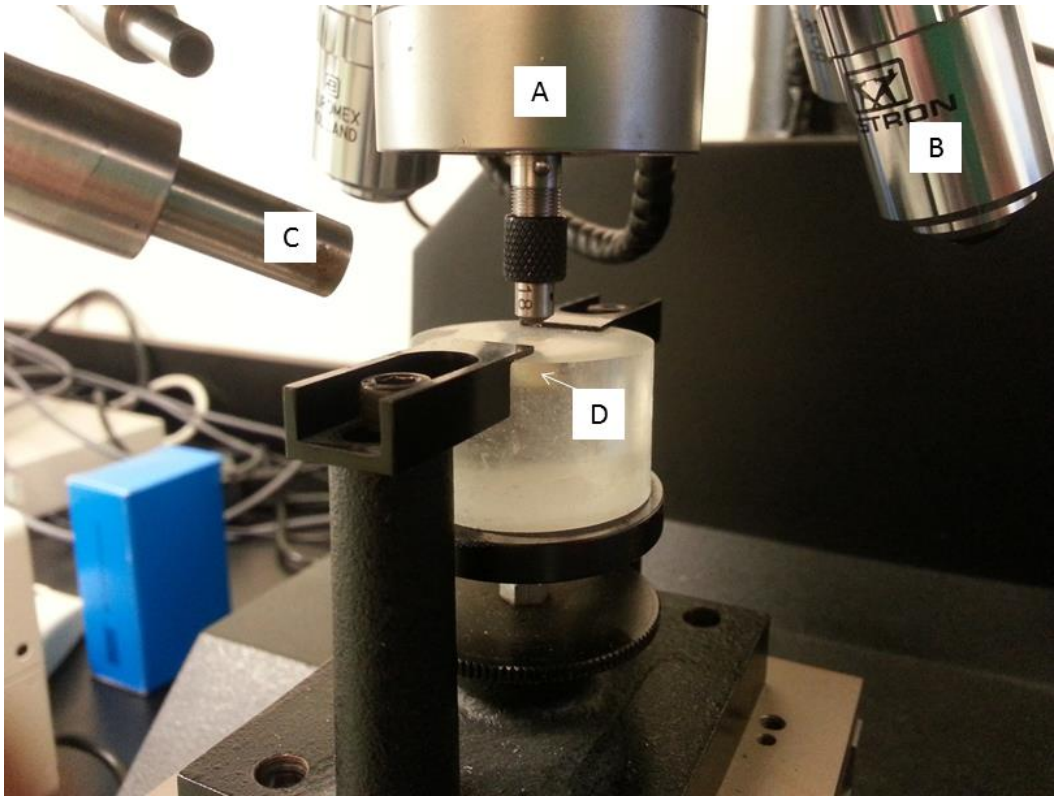

Figure 13 – Wilson Tukon 2100 Microindentation/Vickers Hardness Tester from Instron with silk sample mounted for indentation. (A) Vickers diamond indenter. (B) Microscope lens used for imaging indent in sample. (C) External light source. (D) Silk sample mounted in epoxy.

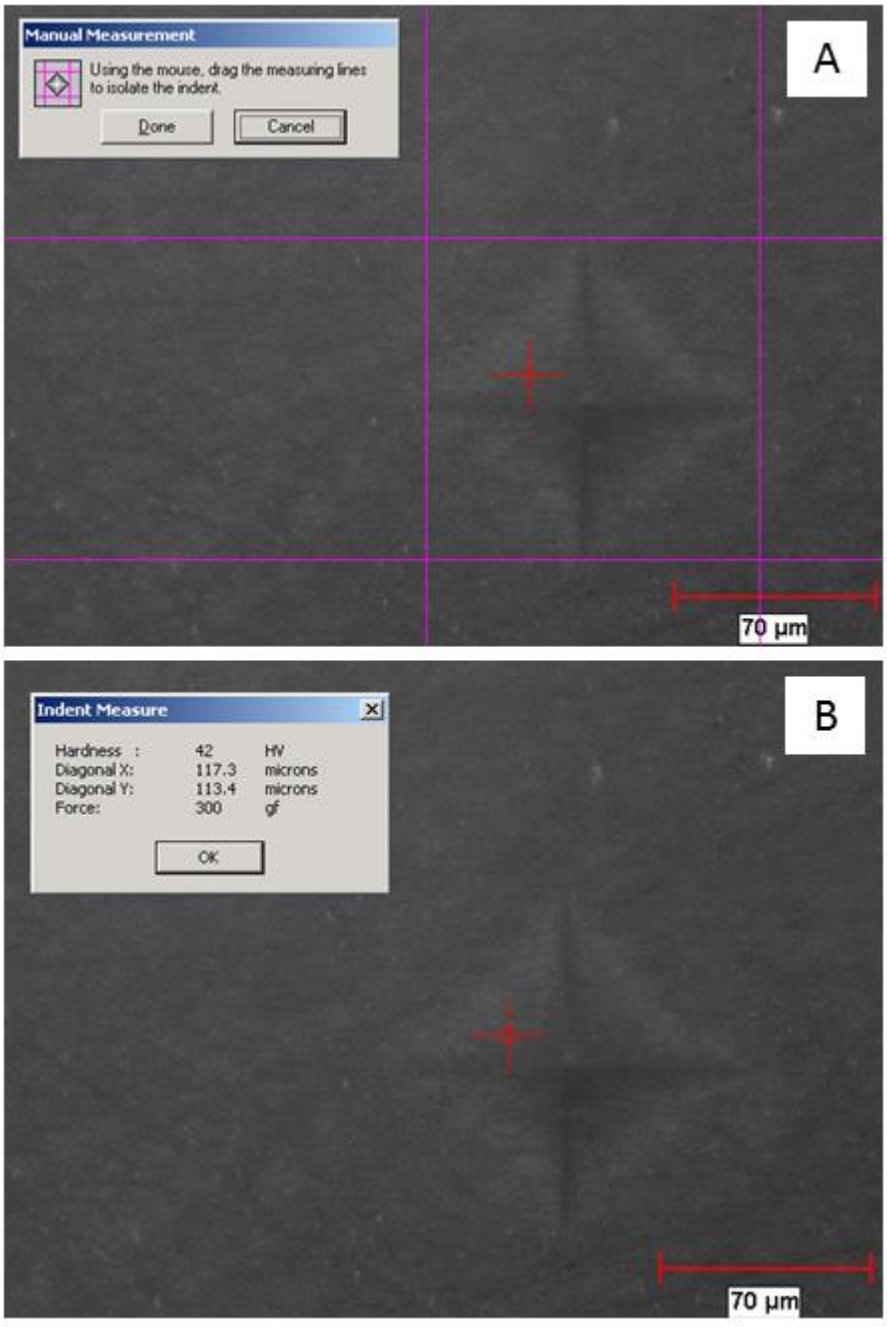

Figure 14 – Wilson-Wolpert Measurement System. (A) Manual measurement tool: the user moves the purple grid lines in order to match the shape of the indent. (B) Automatic report of indent measure including Vickers microhardness number.

In order to check the hardness at different locations, the indenter was started at one edge of the construct and 10 subsequent indentations were made at a spacing

of 0.30 to 0.40 mm from each other and from the edges. Other indentations were made randomly near the edges of the material in order to determine any differences in material properties at different locations along the face of the sample. All hardness values were averaged and reported as an average value and associated standard deviation for each sample.

3.9 Self-tapping capabilities

A human cadaver skull was obtained from Anatomy Gifts Registry (AGR) (Hanover, MD, USA). The skull was fresh recovered by AGR then frozen in order to mimic *in vivo* conditions and screened for all contagious diseases. Serological tests were performed for HIV, HCV, HBV, and Syphilis. The donor was a 59 year old, Caucasian female. Before implantation of the silk screws, the skull was allowed to thaw in a refrigerator for 24 hours. Multiple 1.5 mm pilot holes were drilled with a Synthes (West Chester, PA, USA) Electric Pen Drive on the left side of the skull. Silk screws were then inserted without pre-tapping of the hole. The zygomatic arch and orbital bone were recovered from the skull with a standard hack saw. The hack saw was used to cut to the edge of the bone/screw, bone interface, and then a razor blade was used to delicately separate either side of the bone from the screw. The internal portion of the bone/screw interface was imaged using a digital microscope (Cole-Parmer, Vernon Hills, IL, USA) coupled with an external light source (Kramer Scientific Corporation, Elmsford, NY, USA). Similar implantation techniques were performed on polyurethane bone

mimic and rat cadaver femurs. Polyurethane bone mimic is a rigid foam like material used for testing orthopedic devices.

3.10 Resterilization

Silk samples were autoclaved using a Mark II Controlled Sterilizer (ARES Scientific, Consolidated Stills and Sterilizers, Boston, MA, USA) prior to machining to ensure dimensional stability then 1.5 mm plugs were machined as discussed previously. Six groups of plugs were then autoclaved 1X, 2X, 4X, 6X, 8X, and 10X after machining. For example, 1X samples indicated that the sample was autoclaved once after machining because every sample was autoclaved prior to machining. All groups were tested in double lap shear in dry conditions to test the hypothesis that silk could be resterilized with minimal or no effects on the mechanical properties.

3.11 *In vivo* characterization and implantation technique

All samples were sterilized by autoclaving prior to implantation with a dry cycle at 25 minutes of steam cycle and 15 minutes of drying. Animal studies were conducted under approved protocol #M2010-121 and amendments were approved on June 18, 2012 (#M2010-121 A-1) at Tufts University. For the studies, 250 gram, 15 week old female Sprague Dawley Rats (Charles River Laboratories International, Inc., Wilmington, MA, USA) were anesthetized and the incision area shaven and disinfected with a povidone-iodine scrub. As illustrated in Figure 15, a 5 to 10 mm longitudinal incision was made laterally along the hind limb.

The fascia was separated between the *vastus lateralis* and biceps *femoris* and followed the length of the femur to expose the distal end. A hole with a diameter of 1.5 mm and length of 3 mm was drilled through one of the cortices with a Synthes Electric Pen Drive and the screw inserted into the femur. The incision was closed using a simple interrupted pattern with 5-0 Vicryl suture and overlaid with tissue glue. Material of the same composition but in a simple cylindrical shape was implanted subcutaneously on both sides of the back. Rats were sacrificed at one and four weeks. The femur was removed and the bone sectioned approximately 4 mm from either side of the screw head. The samples were fixed in 10% formalin solution immediately after retrieval then sent to Beth Israel Deaconess Medical Center for histological characterization.

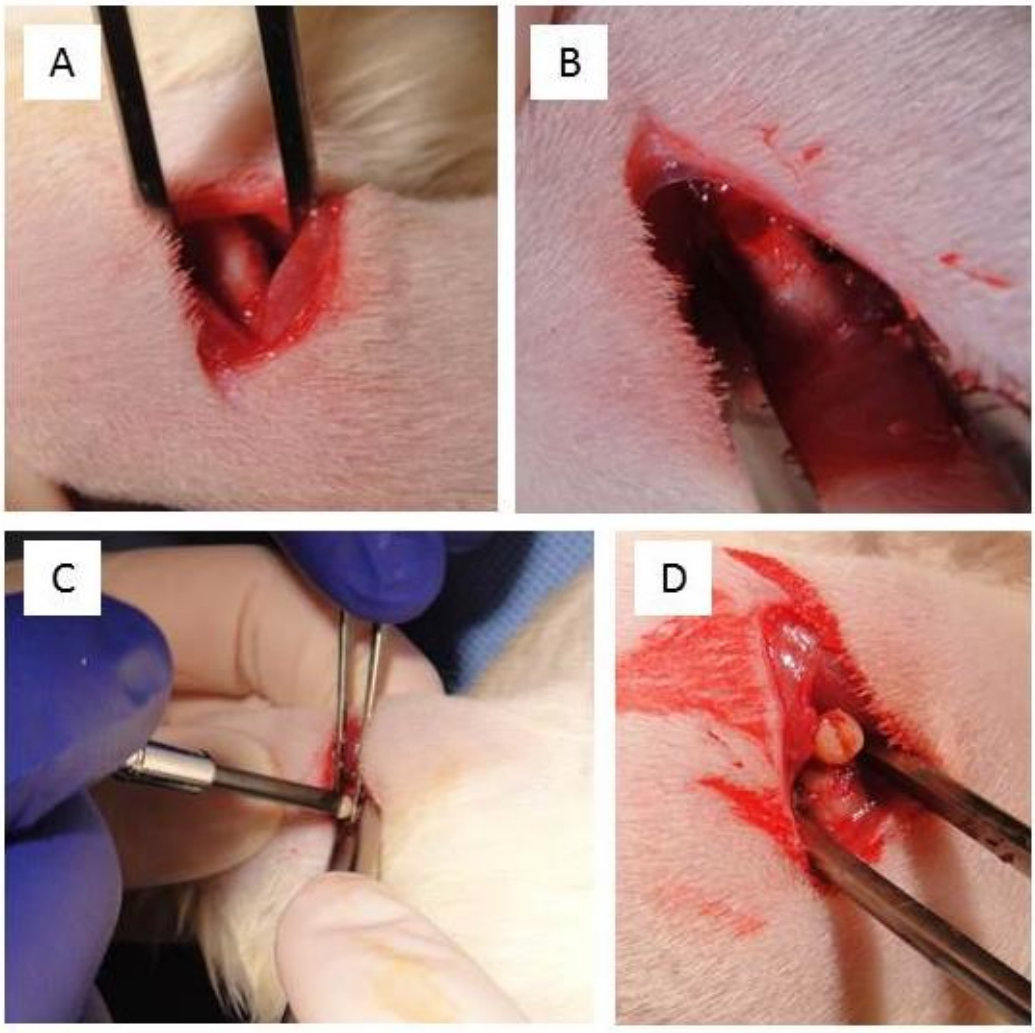

Figure 15 – Implantation technique of silk screw into rat femur model. (A) Exposure of the femur. (B) Pilot hole drilled into femur. (C) Screw inserted into the femur without pre-tapping of the hole. (D) Screw fixed in femur immediately after insertion.

3.12 Statistics

All experiments were run with a minimum of n = 3 for each data point. Statistical analysis was performed with a student-t test, single factor ANOVA, or Wilcoxon ranked sum test to evaluate differences between groups. Differences were considered significant when $p \leq 0.05$ and very significant when $p \leq 0.01$.

Regression analysis was performed using Microsoft Excel (Microsoft, Redmond, WA, USA).

4. Results

4.1 Molding and machining of silk screws and plates

Silk blanks were molded to an average height of 1 inch (2.54 cm) and a diameter of 0.16 in (0.41 cm) after drying resulting in an overall shrinkage of about 47% in diameter. The shrinkage results from the relatively low percentage of silk in solution (25%) as the final construct is close to 100% silk. 25% is the highest percentage of silk in solution without being too viscous for mold filling and without rapid self-assembly of the silk protein. As the samples were simply dried in an oven or fume hood, the deformation can result from uncontrolled air flow, humidity, and temperature; if one side of the sample is more exposed to air, it will dry faster on that side causing a curling effect. The blanks were autoclaved (25 minutes of steam cycle and 15 minutes of dry cycle) for stability then machined into 1-72 machine screw designations (Figure 16A and B) as this was the maximum screw size that could be implanted into a rat femur. Autoclaving was hypothesized to force out any remaining water in the silk samples as well as compact the samples so that there would be no further shrinkage or deformation after machining. Pins were also made of similar dimensions to the major diameter of the 1-72 screws for shear testing. Multiple screw head geometries including slot and Phillips-head were made with the purpose of experimenting with implantation technique. Silk plate blanks were also molded and machined into plates of various thicknesses and shapes. Despite extreme shrinkages and deformations prior to machining, blanks were consistently able to be machined into screws and plates with standard machine tools.

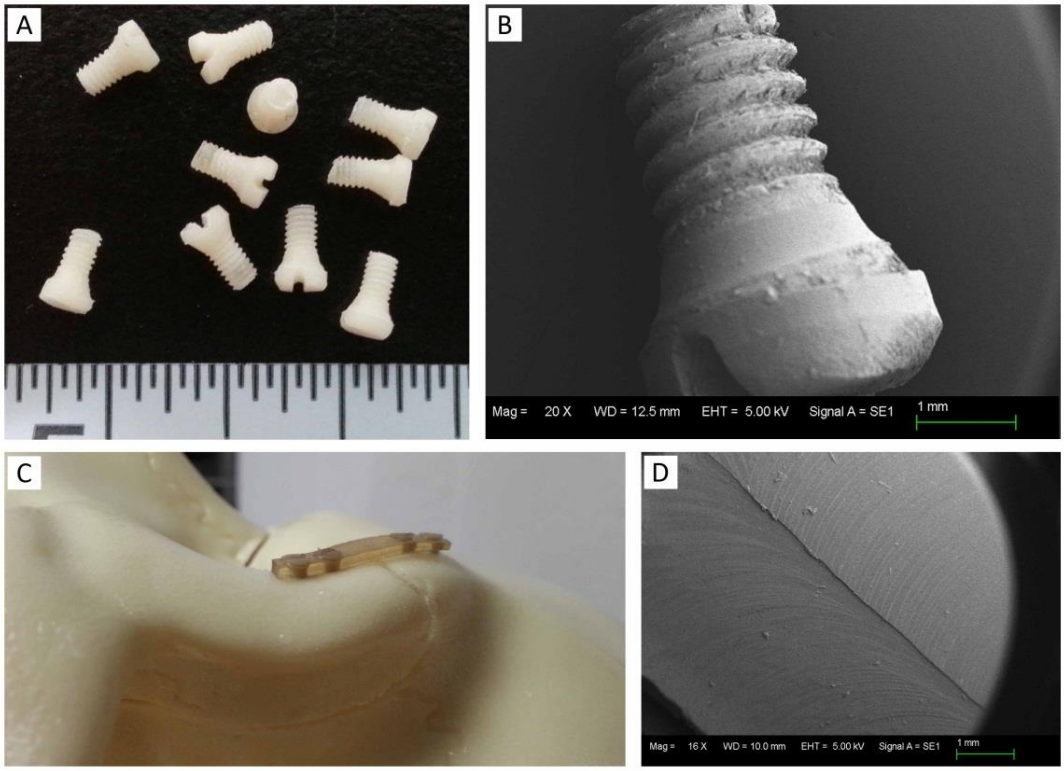

Figure 16 – Initial Silk Screws and Plates. (A) Silk screw (1-72 machine screw designation: major diameter = 0.0730 in; pitch diameter = 0.0640 in; minor diameter = 0.0560 in). (B) SEM image of 1-72 silk screw at 20X. (C) Combination of silk screws and plates on model skull orbital bone to show fixation potential. (D) SEM image of milled surface of silk plate at 16X.

4.2 Structure and morphology

Fourier transform infrared spectroscopy (FTIR) showed significant β-sheet crystalline fractions in the screw blanks. As shown in Table 5, the spectra exhibited a distinct peak at 1621 cm^{-1} which is characteristic of β-sheet rich silk materials and deconvolution showed a of β-sheet content of 49.3 ± 3.6% in the silk screws. Scanning electron microscope (SEM) images showed a smooth surface finish (Figure 16D) after machining with the lathe or mill and the ability to make reproducible geometries. The screw threads were machined by hand with a standard 1-72 thread die so the cutting surface is not as smooth as a milled or

lathed surface (Figure 16B). The surface roughness could be attributed to detached silk material that was not properly removed from the screw threads or due to the inconsistency of cutting threads by hand. Besides the surface roughness of the screw threads, the silk screws were very geometrically reproducible between and within different batches of silk.

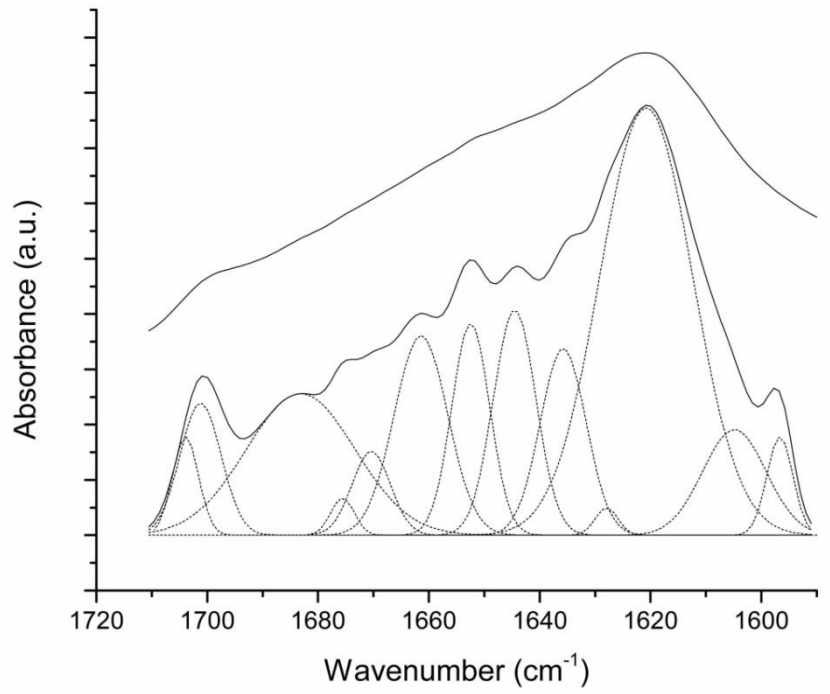

Conformation	Average (%)	Standard Deviation (%)
Side	6.94	3.03
Beta Sheet	49.31	3.64
Random Coil	15.15	2.26
Alpha Helix	10.75	4.71
Turns	17.85	6.68

Table 5 – FTIR spectroscopy of silk samples. Measurements represent the average of 64 scans taken at a resolution of 4 cm^{-1}. Peaks at 1621 cm^{-1} indicate beta sheet conformation while peaks at 1640 cm^{-1} indicate random coil conformation. The inserted table provides the quantitation of the spectra using deconvolution.

4.3 Swelling properties and water uptake

The swelling ratio and water uptake (%) were determined for the silk screws. The swell ratio and water uptake (%) were measured for both non-autoclaved and autoclaved samples to determine differences. Non-autoclaved screws had a swell ratio of 0.65 +/- 0.02 and a water uptake of 39.5 +/- 0.9 %. Autoclaved screws produced a swell ratio of 0.38 +/- 0.04 and a water uptake of 27.6 +/- 2.0 %. All samples were evaluated with n = 3. Differences between swell ratio and water uptake of non-autoclaved and autoclaved samples were considered statistically significant ($p < 0.01$).

4.4 Mechanical properties

Shear forces are one of the most prominent forces experienced in osseous-fixation devices. Pure silk pins were tested to determine the maximum shear stress. The 0.059 in (1.5 mm) pins were tested in shear in non-hydrated conditions. The silk pins achieved a maximum shear stress of 104.21 ± 0.43 MPa (n = 3). The pure silk pins were consistent in terms of mechanical properties, as shown by the small standard deviation, during dry double lap shear testing and achieved a comparable maximum shear stress to PLGA. PLGA screws composed of 82:18 or 80:20 PLA:PGA achieve a maximum shear stress of roughly 100 MPa [52, 57]. However, the limitations of the current silk format include hydrated mechanical strength, as strength significantly decreased when hydrated. Pins were machined to 1.49 ± 0.01 mm (1.50 mm) diameters but swelled to 1.75 ± 0.02 mm diameters after hydration ($p < 0.01$). The pins achieved a hydrated maximum shear stress of

15.30 ± 3.38 MPa (n = 3). The difference between dry and hydrated shear strength was significant with $p < 0.01$.

The silk screws (1-72 designation) were tested in non-hydrated and hydrated conditions for pull-out strength. The artificial polyurethane bone was drilled with a 0.059 in (1.5 mm) drill bit but was not tapped as the screws were self-tapping. In the non-hydrated state, the screws exhibited a maximum load of 37.81 N ± 28.82 N (n = 6). All screws pulled-out of the artificial bone and the threads appeared undamaged. In the hydrated state, the screws achieved a maximum load of 19.18 ± 5.98 N. Four of the screws pulled out of the artificial bone while two fractured below the screw head. The variability between results shows that more consistent threads and major diameters need to be produced to obtain accurate results from pull-out strength testing. Further, the silk screw threads were machine screw designation so they are not tailored for fixation in bone.

4.5 Dimensional stability after autoclaving

Samples need to be sterilized before *in vivo* implantation, and, thus, the effect of autoclaving was analyzed. The effect of autoclaving was already analyzed on the swelling properties but now the focus is on dimensional stability. Screws were made without autoclaving of the blanks prior to machining and measurements were taken of mass, major diameter, overall height, and head diameter before the first autoclave cycle, after the first autoclave cycle, and after the second autoclave cycle. There was shrinkage in all aspects of the screw due to the first autoclave

cycle, with a loss of 2.13 ± 0.31% in mass, 1.14 ± 1.01% in major diameter, 2.99 ± 1.84 % in overall height, and 2.07 ± 0.92% in head diameter. A 1-tailed paired t-test showed that the mass, overall height, and head diameter showed significant differences from the initial measurements ($p < 0.05$); the difference in major diameter was not significant with $p = 0.09$. After the second autoclave cycle, the changes were negligible as there were both gains and losses in the dimensions and mass of the screws depending on the sample. The variability can be attributed to measurement technique and human error. There was a change of -0.02 ± 1.01% in mass, -0.19 ± 0.38% in major diameter, -0.14 ± 0.38% in overall height, and -0.42 ± 0.49% in head diameter. The negative percentages indicate that the samples actually enlarged or gained mass after the second autoclave cycle. A 1-tailed paired t-test was run and all p-values for differences between the first and second autoclave cycle were greater than 0.09 indicating that no differences were significant. These results show that the first autoclave cycle has an effect on the properties of the material such as mass and dimensional losses. For all future manufacturing and testing, all samples will be autoclaved once prior to machining to ensure dimensional stability then once after machining for sterilization to mimic implantation conditions.

4.6 Protease XIV *in vitro* degradation

4.6.1 Percent mass loss

In vitro degradation was observed in the silk samples incubated in 5 U/ml of Protease XIV. The samples were 0.059 in (1.5 mm) cylindrical geometries of

similar sizes to the shanks of 1-72 machine screws with the goal of correlating *in vitro* enzymatic degradation to *in vivo* resorption of the screw shank in the bone. As shown in Figure 17, there was 31% mass loss after 23 weeks of incubation. All differences between mass loss of the PBS control and protease incubated samples were considered significant for all time points (1, 4, 8, and 23 weeks) with a p-value ≤ 0.05. However, as shown by Table 6, the percent mass loss per day differed between the different time points. Between 1 and 8 week time points, the % mass loss steadily increased from 0.22% to 0.30% mass loss per day. However, over the 23 week time point, the % mass loss decreased to 0.20% mass loss per day. While no conclusions can be made definitively, this may indicate that the silk material degrades slower after a specific point. This could be due to differences in the material at different distances away from the central axis. However, there may be experimental errors such as loss of activity of Protease XIV due to freeze and thaw cycles or inactive enzyme caked onto the silk samples. If inactive enzyme is coating the sample, it may not allow for active protease to bind to and degrade the sample.

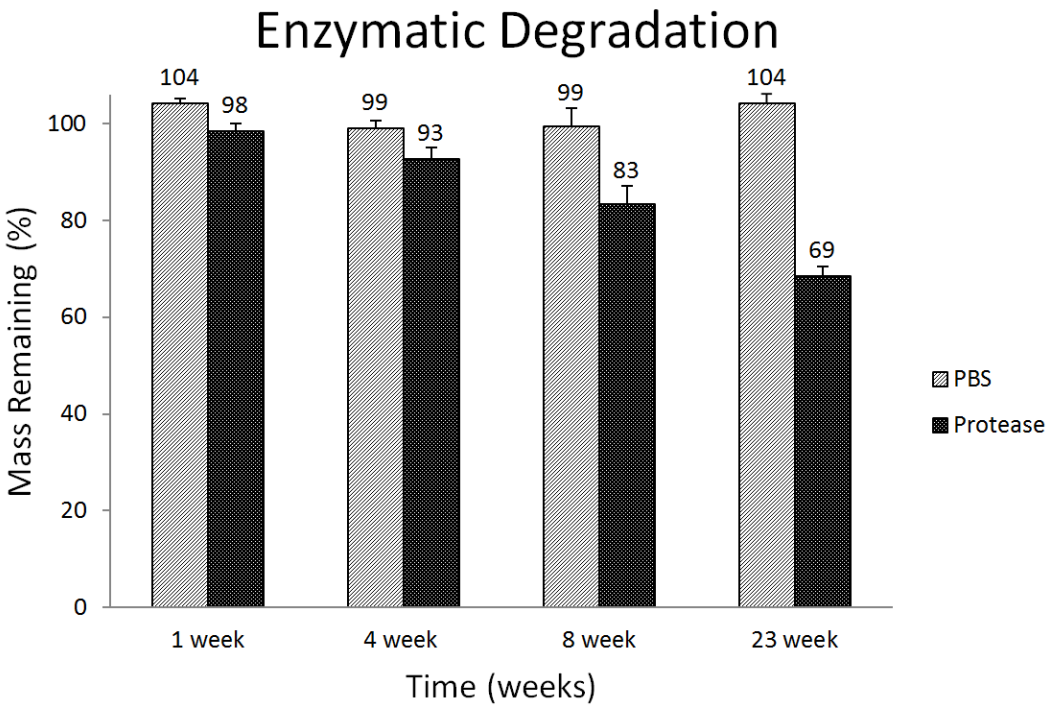

Figure 17 – Percent mass remaining of silk screw material as a function of time in PBS and in 5.0 U/ml protease. All differences between the control and enzymatic degradation are considered significant ($p \leq 0.05$) for all time points.

Table 6 – Percent mass loss per day for 1, 4, 8, and 23 week time points of enzymatic degradation.

Time point	**% Mass loss per day**
1 week	0.22
4 week	0.26
8 week	0.30
23 week	0.20

4.6.2 SEM confirmation of degradation by surface erosion

SEM images, as shown in Figure 18 – Figure 23, were used to confirm the results of *in vitro* proteolytic degradation. Control (PBS) samples and samples incubated in Protease XIV for 1, 4, 8, and 23 weeks were imaged. Master control samples

were simply machined then stored in ambient conditions prior to imaging to use as a control for the PBS control samples. All samples incubated in protease showed surface erosion as compared to their controls; this is expected as silk fibroin has been reported to degrade by surface erosion [54].

Figure 18 shows a silk sample that was only machined but never soaked in PBS. This sample will be used as the master control sample as both PBS controls and Protease XIV incubated samples can be compared to determine degradation by surface erosion. Almost the entirety of the machining surface appears smooth but there are some minor surface defects in the sample. These can be attributed to poor machining technique or material defects.

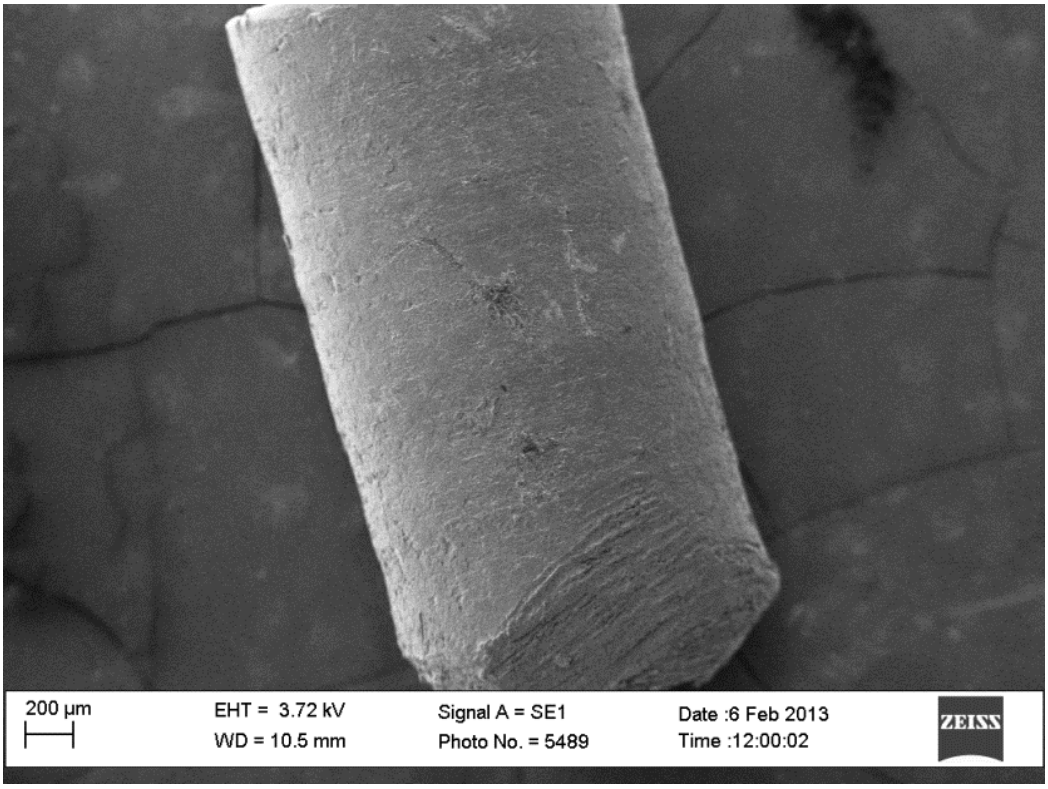

Figure 18 – Master control silk sample. This sample was machined on a lathe but never soaked in PBS.

Figure 19 compares all PBS control samples from 1, 4, 8, and 23 weeks. All samples are comparable to the master control sample and none of the samples incubated in PBS showed any significant signs of surface erosion consistently across all samples. Thus, silk samples did not degrade in a PBS solution as confirmed by the mass loss percentages and visual SEM characterization. While the samples showed no degradation by mass measurements or imaging of surface erosion, future tests need to be done to determine if soaking the silk material in PBS has an effect on mechanical properties over time.

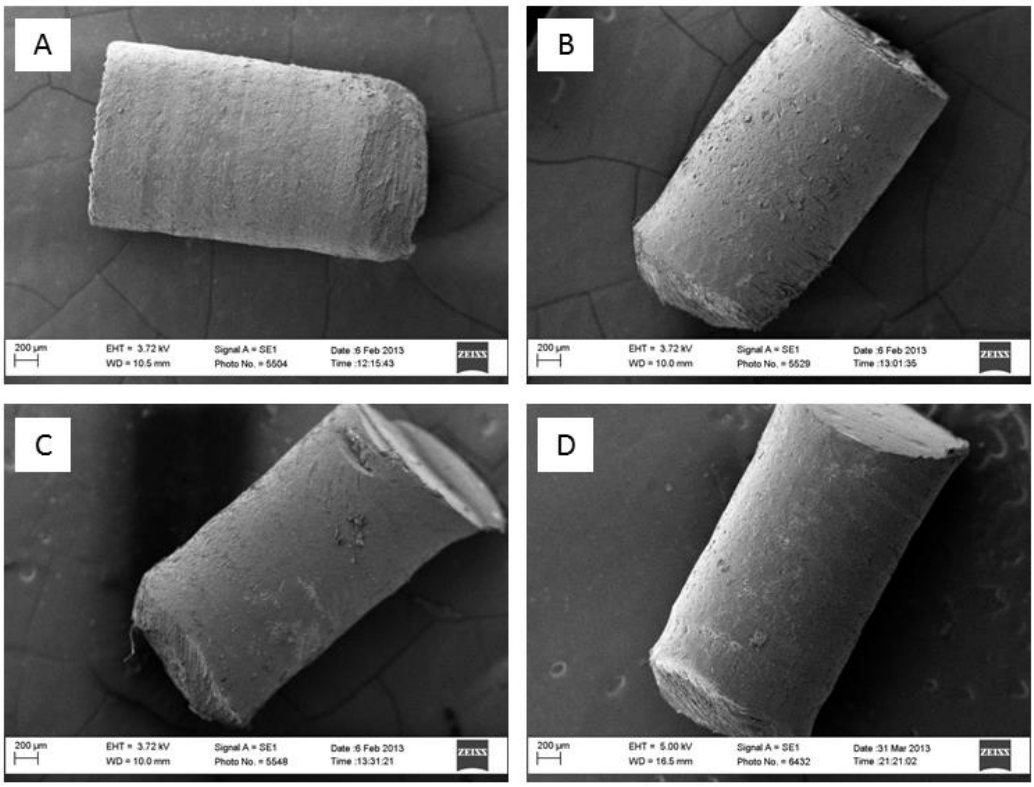

Figure 19 – (A) 1 week PBS control. (B) 4 week PBS control. (C) 8 week PBS control. (D) 23 week PBS control.

Figure 20 depicts the silk samples after 1 week of incubation *in vitro*. Samples incubated in enzyme, Figure 20B and D, show surface erosion of the silk material

compared to the PBS control samples. While some of the surface characteristics of images B and D can be attributed to dried protease, the samples were washed thoroughly to make sure minimal protease was remaining on the samples upon weighing and imaging. Further, the mass loss percentages confirm the preliminary degradation of the silk material.

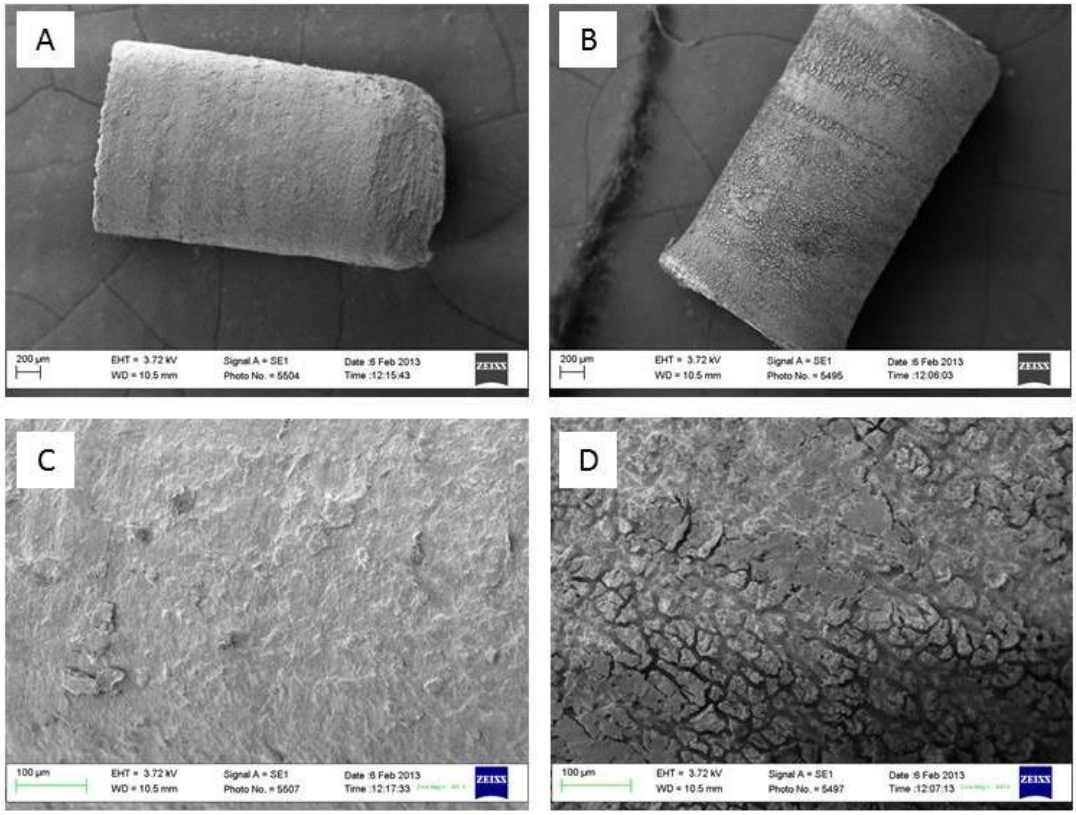

Figure 20 – (A) 1 week PBS control at low magnification. (B) 1 week Protease XIV at low magnification. (C) 1 week PBS control at high magnification. (B) 1 week Protease XIV at high magnification.

Figure 21 shows samples incubated for 4 weeks in PBS and Protease XIV. The samples incubated in enzyme, Figure 21B and D, show much more obvious signs of surface erosion as compared to both the control samples and the 1 week samples. Significant pitting of the surface is seen and can be confirmed by the mass loss percentages as degradation of the material. The PBS control sample's

surface does not appear as smooth as some other control samples but the surface does not appear to be eroded in any way similar to the protease samples. Thus, the surface defects may be attributed to material defects or poor machining technique.

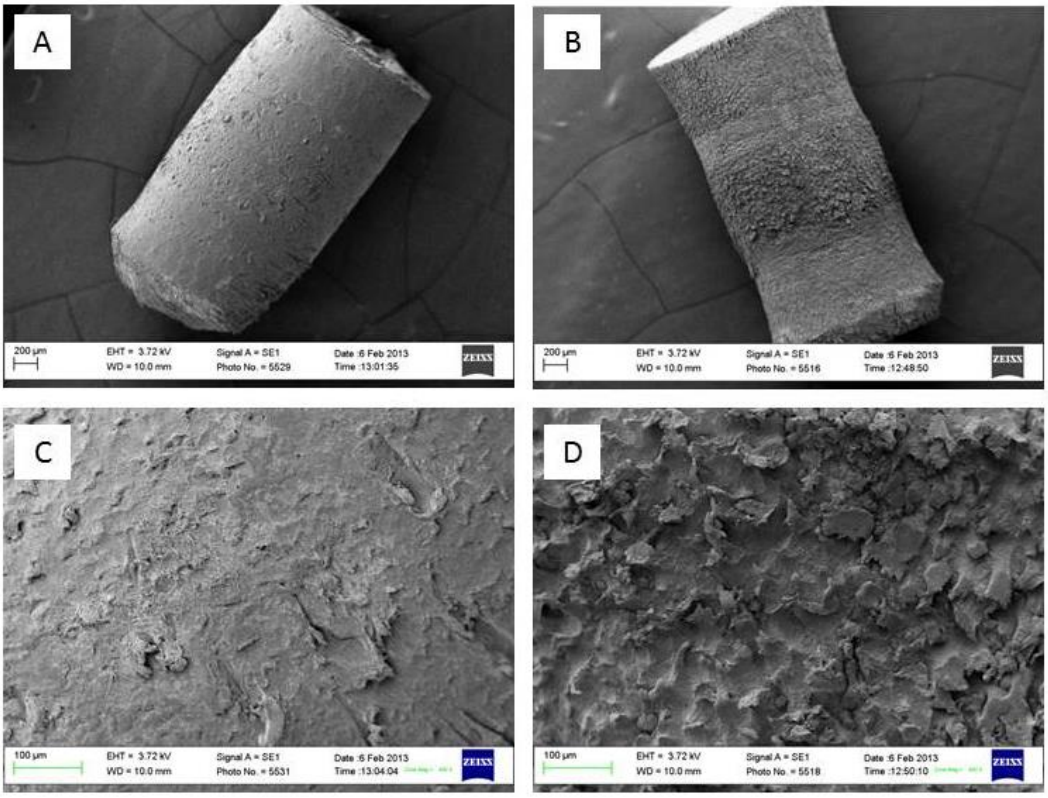

Figure 21 – (A) 4 week PBS control at low magnification. (B) 4 week Protease XIV at low magnification. (C) 4 week PBS control at high magnification. (B) 4 week Protease XIV at high magnification.

Figure 22 represents silk samples after 8 weeks of incubation. The surface erosion of the samples incubated in enzyme is much more noticeable as compared to 1 and 4 week samples.

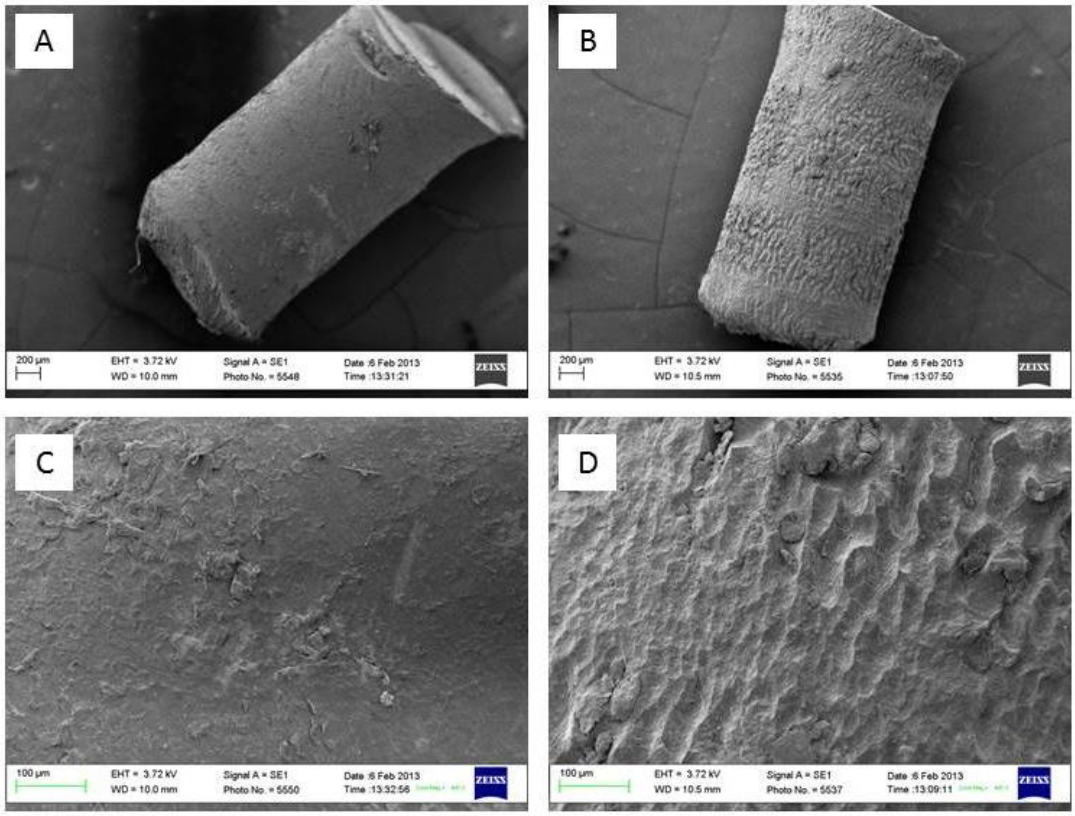

Figure 22 – (A) 8 week PBS control at low magnification. (B) 8 week Protease XIV at low magnification. (C) 8 week PBS control at high magnification. (B) 8 week Protease XIV at high magnification.

Figure 23 depicts silk samples incubated for 23 weeks. The control samples do not appear to have any signs of surface erosion; however, the samples incubated in Protease XIV do not show similar pitting as compared to the shorter time points. The samples look as if they have been eroded and even smoothed by the enzyme similar to how sand can smooth rock; the samples even look smoother compared to control samples and the master control sample. This could occur due to the increased rinsing cycles of a longer time point sample as more rinsing could smooth the surface of the construct. Also, there could be differences in material properties closer to the central axis of the cylinder. Nevertheless, the samples

incubated in enzyme are visibly smaller than their PBS counterparts and the mass loss confirms continued degradation of the silk samples.

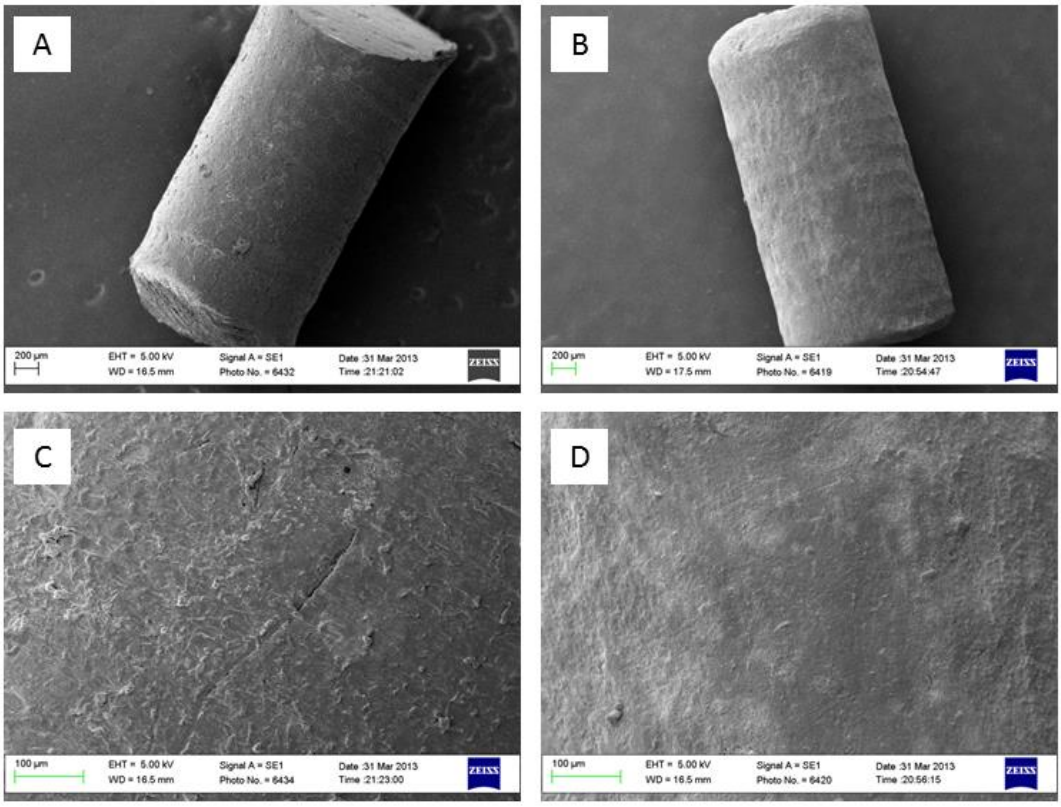

Figure 23 – (A) 23 week PBS control at low magnification. (B) 23 week Protease XIV at low magnification. (C) 23 week PBS control at high magnification. (B) 23 week Protease XIV at high magnification.

4.7 Vickers microhardness

Silk samples were evaluated for Vickers microhardness with a 300 gram force load (Hv0.3) with $n \geq 10$ per sample. Table 7 indicates the hardness numbers and standard deviation for each sample. A single factor ANOVA yields a p-value of 0.25 indicating no significant differences between groups. The average Hv value for all samples was 40 kg/mm^2. Because the variances were relatively small and the statistical analysis yielded no statistical significance between groups, an Hv =

40 kg/mm^2 is an accurate value for the microhardness of this silk material format. The minimum Hv value obtained for all tests was 34 kg/mm^2 and the maximum was 46 kg/mm^2, yielding a range of 12 kg/mm^2. However, most samples fluctuated between 38 and 42 kg/mm^2.

Table 7 – Summary table of Vickers microhardness for three silk samples.

Groups	*n*	*Average Hv (kg/mm^2)*	*Standard deviation*
Sample1	36	39.75	2.63
Sample2	20	40.65	1.93
Sample3	14	40.79	2.22

Figure 24 shows a representative image of the silk surface before and after indentation with a Vickers diamond indenter with 300 gram force load applied for 3 seconds and allowed to dwell for 10 seconds. All samples were analyzed immediately after indentation neglecting any potential indentation recovery effects often seen in softer polymeric materials [58].

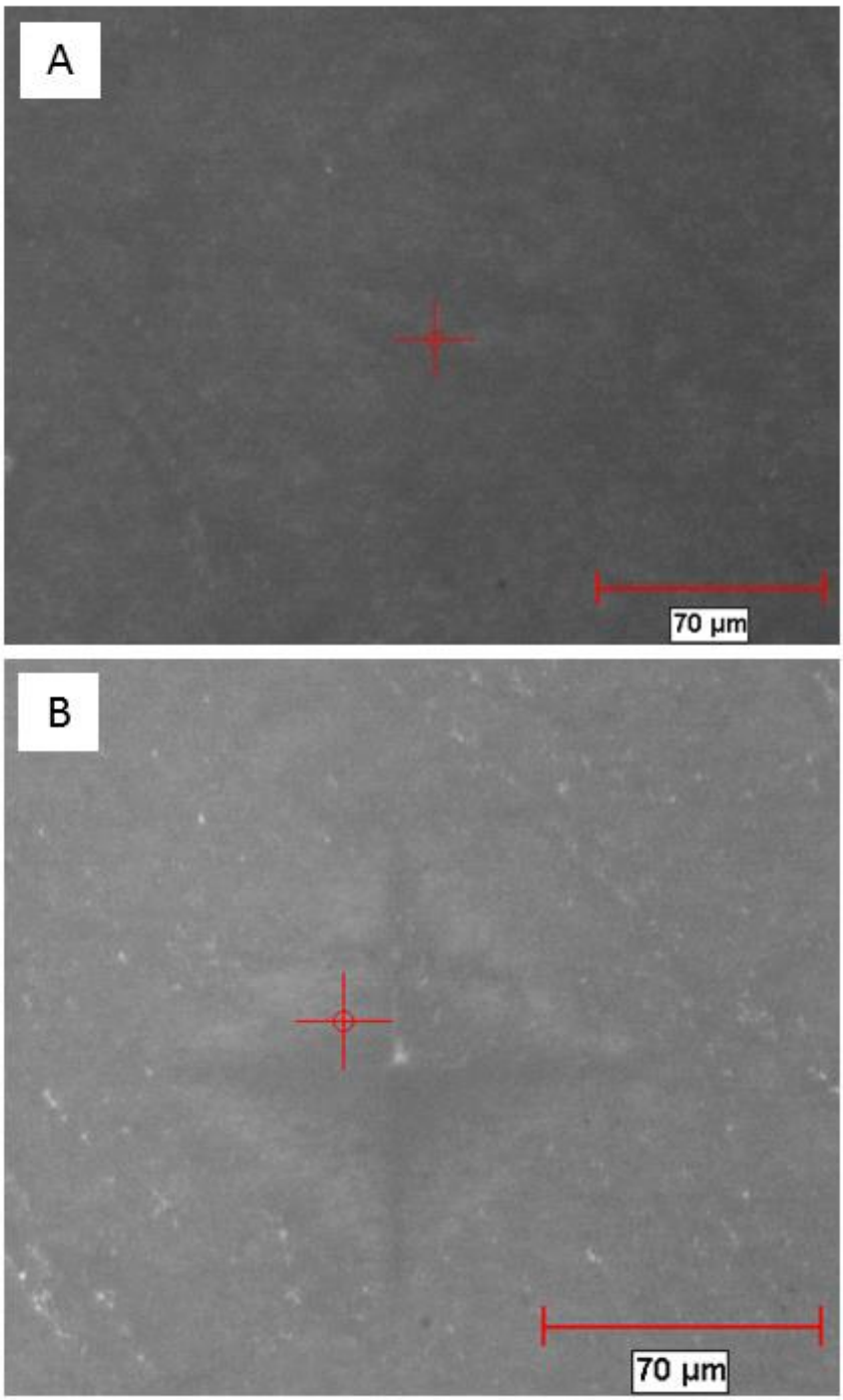

Figure 24 – Vickers microhardness testing of silk samples. (A) Silk surface prior to indentation. (B) Silk surface after indentation with a Vickers diamond indenter with a 300 gram force load applied for 3 seconds and allowed to dwell for 10 seconds.

4.8 *In vitro* implantation technique and self-tapping capabilities

4.8.1 Implantation in full skull polyurethane model

Because one of the main problems with current resorbable devices is the implantation technique, the implantability of the silk screws and plates was studied. Current resorbables are at a disadvantage compared with metallic devices as they require a two-step implantation process of careful pre-drilling and pre-tapping of the pilot hole. Further, the plates require a time dependent heating step and molding to the exact curvature of the boney interface. Thus, silk screws were tested to examine self-tapping capabilities and plates were examined for *in situ* molding technique. These processes were done simultaneously in order to recreate a real CMF reconstruction.

Once dry, the silk plates were malleable again by spraying a mist of water on the surface. To test implantation, as shown in Figure 25, a Sawbones full skull model's (Item #: 1345, Vashon, WA, USA) orbital fracture was fixed with a 4-hole 100% silk screw and plate system. The implantation technique involved: 1) Spray the plate with water to allow shaping 2) Use the plate as a guide to drill holes into the bone 3) Insert the screw without pre-tapping of the hole.

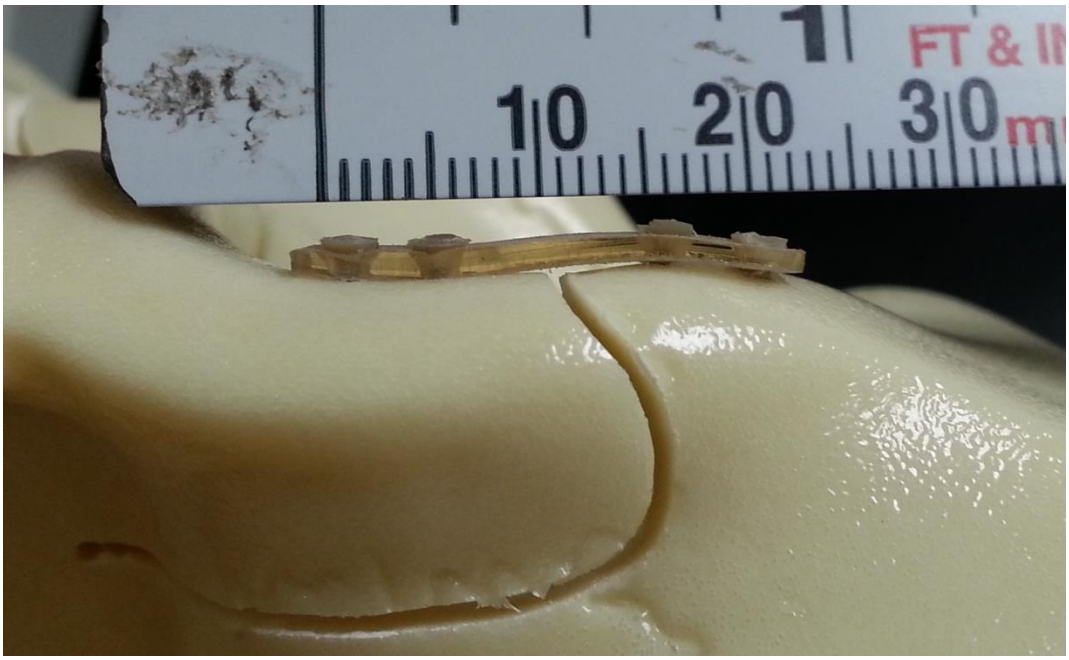

Figure 25 – 100% silk screw and plate system installed on a mock skull model. The implantation technique involved: 1) Spray the plate with water to allow shaping. 2) Use the plate as a guide to drill holes into the bone. 3) Insert the screws without pre-tapping of the hole.

4.8.2 Self-tapping capabilities in rat cadaver femurs

Self-tapping capabilities of silk screws were tested on cadaver rat femurs to experiment with implantation technique for the animal model (Figure 26). A 1.5 mm pilot hole was drilled with the Synthes Electric Pen Drive and silk screws were inserted without pre-tapping of the hole. Minimal axial compression was required for insertion and it felt as if the threads were grabbing onto or cutting into the bone, pulling the screw downward into the bone.

Figure 26 – 1-72 silk screws inserted into cadaver rat femurs. The yellow circles denote the location of the silk screws in the femurs.

4.8.3 Self-tapping capabilities in human cadaver skull

The specific application for the silk screws and plates are CMF procedures. Although polyurethane bone mimic and rat femurs may be similar to the properties of human bone, they are not identical. Silk screws of various different lengths were inserted into the different pilot holes. Many screws were able to be fully inserted into the pilot hole while some screw heads fractured upon insertion. However, most fractures occurred when the screw threads were inserted most, if not all of the way into the bone. In Figure 27C (white circle), one can see the fractured head of silk screw inserted into the orbital bone. Further testing needs to

be done with better head geometries and bone screw threads, rather than machine screw threads, to truly test the self-tapping capabilities of the silk screws.

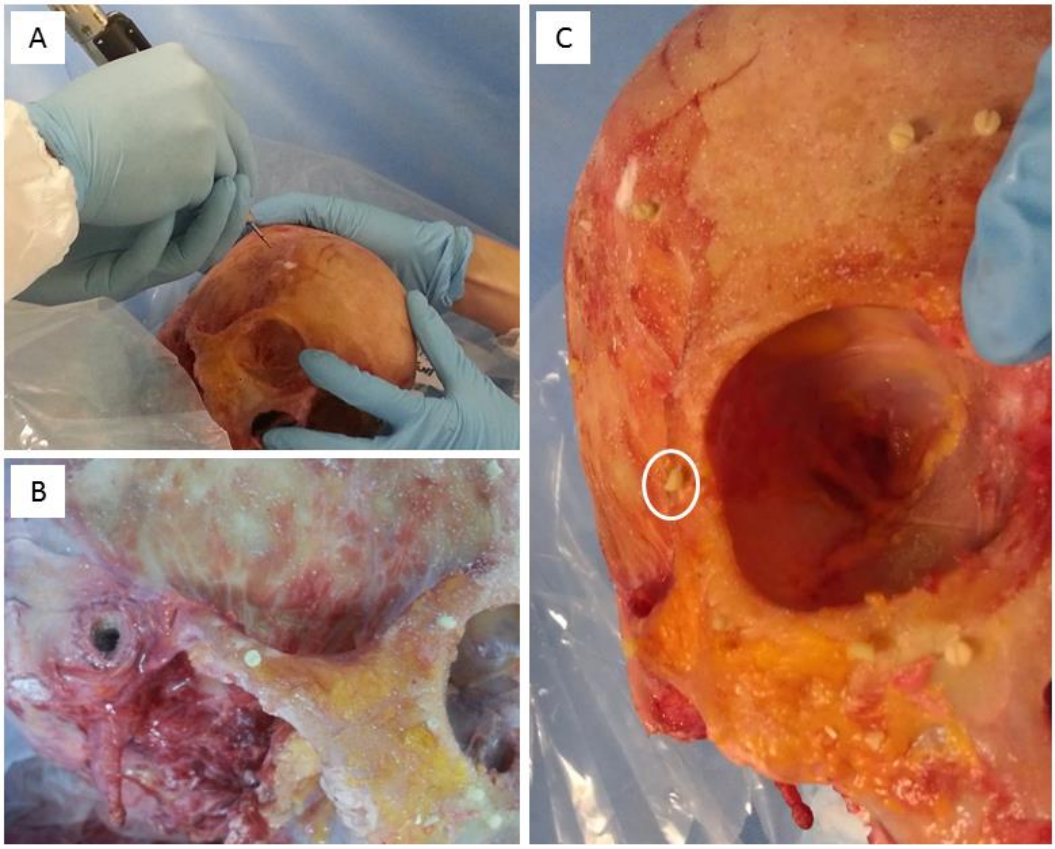

Figure 27 – Implantation technique of silk screws in a human cadaver skull. (A) 1.5 mm pilot holes drilled into multiple locations with a Synthes Electric Pen Drive. (B) 1-72 silk screw inserted into the zygomatic arch. (C) Silk screws inserted into various different locations in the skull.

Nevertheless, the silk screws showed promising utility as self-tapping devices as the majority of the screws were able to be inserted into the human cadaver skull. Figure 28 and Figure 29 depict the internal section of the bone/screw interface; the screw was removed prior to imaging but the orientation of the image is as if the screw was inserted perpendicular to the scale bar. In both images, the higher magnification picture focuses on visible threads cut into the upper portion of the pilot hole. The threads appear to be left-handed threads despite being machined

with a right-handed die. Most likely, the screw was inserted at an angle causing it appear as if it is a left-handed thread.

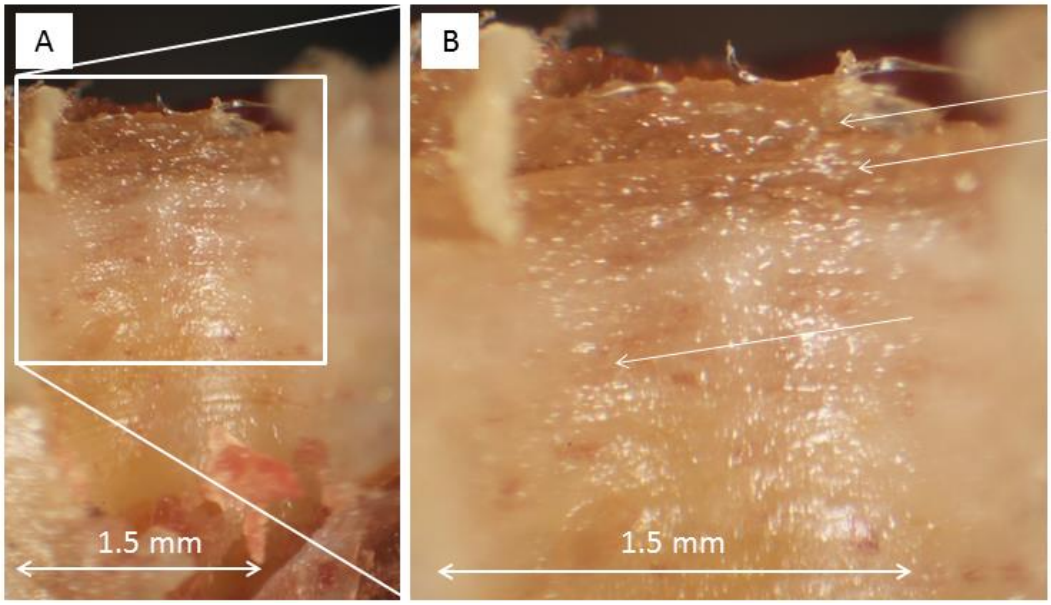

Figure 28 – Cross section of the bone screw interface after insertion of silks screw in the zygomatic arch. Both images show helical cuts as well as visible striations in the bone most likely due to screw insertion. (A) Low magnification. (B) High magnification.

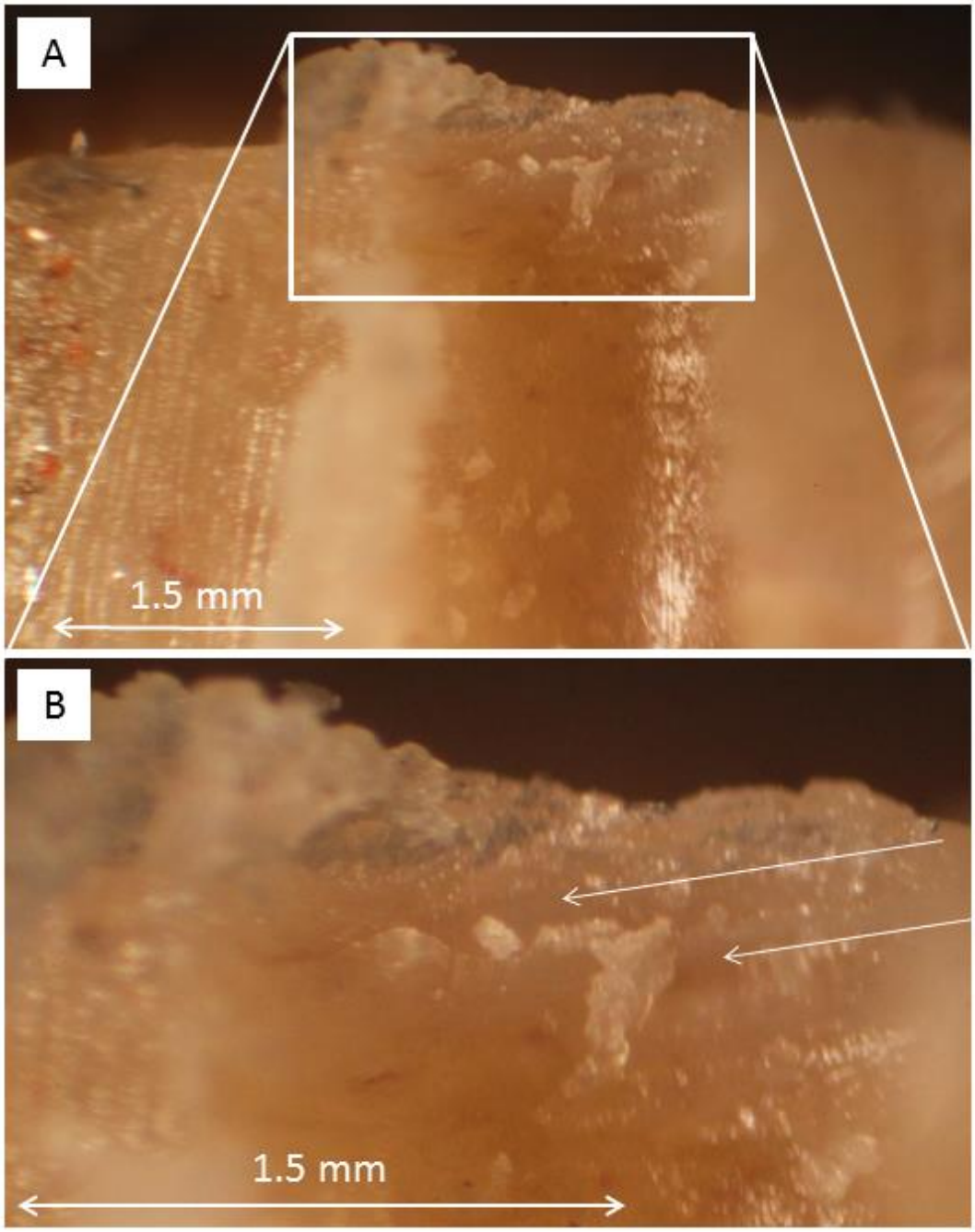

Figure 29 – Cross section of the bone screw interface after insertion of a silk screw in the orbital bone. (A) Low magnification. (B) High magnification shows two helical cuts in the bone.

Certain conditions that may have affected the insertion of the screws include patient age, health, sex, and bone hydration [50, 59-61]. The bone hydration state upon freezing may affect the insertion of the screws; the microhardness of dry

bone increases by 30 – 40% as compared to fresh bone [49, 50]. If frozen then thawed bone is less hydrated than living bone, the screws may be harder to insert due to increased hardness of bone when less hydrated [61]. Table 8 shows the effect of storage conditions on the microhardness of bone. The cadaver skull used for this experiment was stored at -20°C and then thawed prior to testing. Because the "Fresh" bone hardness is very similar to the "Dry Sealed for Forty-eight Hours at -20 Degrees Centigrade" bone, the cadaver skull used for this experiment may be a very good mimic for *in vivo* implantation conditions because it was stored at -20°C prior to testing. Thus, the fact that the silk screws showed self-tapping potential is a very good sign.

Table 8 – The effects of storage conditions on the microhardness of bone. The mean of ten indents were taken on the freshly prepared surface of interstitial bone. [50]

Specimen's Location, Age (*Years*), Sex	Fresh	Dry Sealed for Forty-eight Hours at –20 Degrees Centigrade	Dried at 60 Degrees Centigrade for Twelve Hours	Embedded in Methyl Methacrylate	10 Per cent Neutral Formalin for Twenty-four Hours	Normal Saline Solution at 4 Degrees Centigrade for Twenty-four Hours
Fibular diaphysis, 35, M	56.1	54.6	85.2	83.2	79.0	44.1
Fibular diaphysis, 35, F	54.0	53.8	83.1	79.6	68.1	42.0
Tibial diaphysis, 12, M	29.2	31.0	69.4	38.7	38.1	24.1
Fibular diaphysis, 20, M	47.3	46.2	81.0	57.2	60.5	39.4

4.9 Resterilization: effect of autoclaving on mechanical properties

One of the cost-benefits to using metallic bone screws is the ability to resterilize and reuse devices that were not needed for a specific surgery. For example, a device could be opened in the operating room but never implanted. This device would be classified as non-sterile and would need to be resterilized. Current

resorbables, such as PLGA, cannot be resterilized or reused. Thus, silk samples were tested mechanically to determine the effect of resterilization (autoclaving) on the mechanical properties (maximum shear stress). Figure 30 shows the effect of autoclaving on maximum shear stress (MPa) after 1, 2, 4, 6, 8, and 10 autoclave sterilization cycles. The number of autoclave cycles indicates the number of cycles post-machining as all samples were autoclaved once prior to machining. A single factor ANOVA showed that there was significance between groups with a p-value < 0.01. Nevertheless, the silk device may retain clinically relevant strength even after 10 autoclave cycles.

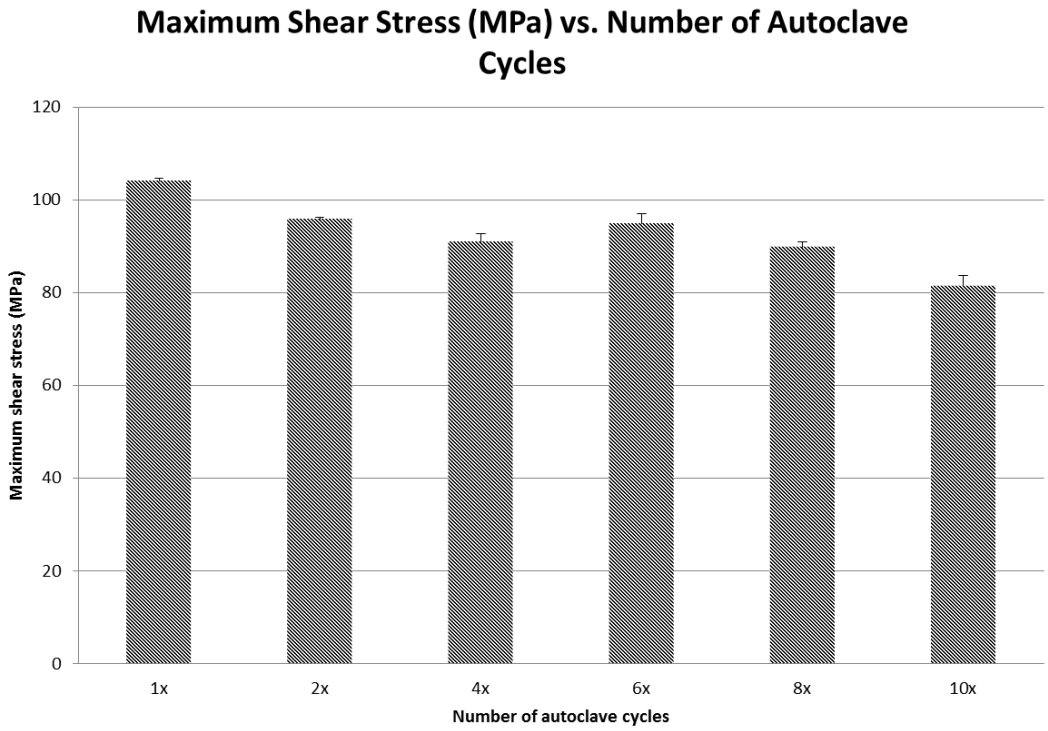

Figure 30 – Maximum shear stress (MPa) versus number of autoclave cycles for 1.5 mm silk pins. The number of autoclave cycles indicates the number of cycles post-machining as all samples were autoclaved once prior to machining.

4.10 *In vivo* characterization in a rat femur model

4.10.1 Implantation technique and post-surgical assessment

Immediately after surgery, after the effects of anesthesia diminished, the rats were mobile on all four legs and were able to rear up on their leg containing the screw. While this could be attributed to the lingering effects of anesthesia or the pain medication, the rats were examined for 3 – 4 days post-surgery and remained mobile on all four legs.

Throughout the 4 week period, the rats were mobile on all four legs without showing any visible signs of pain, discomfort, or distress. Two animals experienced wound dehiscence but were treated with the antibiotic Baytril (commonly used antibiotic for bacterial infections in animals); the wound closed by itself and did not need further attention. Explants were isolated and characterized with photographs (Figure 31) to show that the screws did not back out of the bone and there were no macroscopic visible negative reactions. One screw showed soft tissue encapsulation; this was determined to be from implantation technique as some soft tissue could get caught around the screw head when screwed into the bone. No other animals showed soft tissue encapsulation so this result is not expected to be an issue moving forward. For future studies, the screws will be inserted more carefully making sure not to disrupt the surrounding soft tissue.

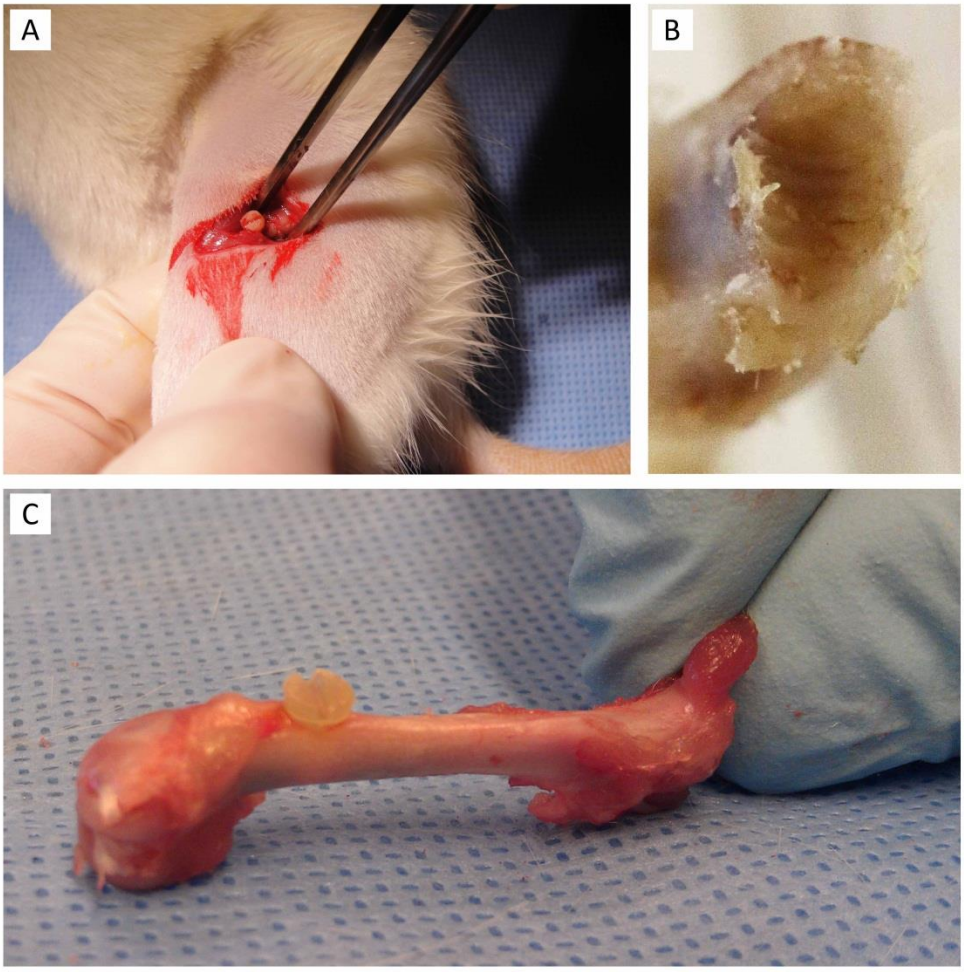

Figure 31 – *In vivo* implantation of pure silk screws. (A) Implantation of silk screw. (B) Cross-sectional photograph of the rat femur showing imprints or cuts of screw threads in the bone. (C) Silk screw and bone interface after 4 weeks *in vivo*. Screw did not back out and remained fixed in the femur.

4.10.2 Histological characterization of silk screw implants in rat femurs

Biocompatibility refers to the host response elicited by a material. Tissue reactions can be numerous and complex but local tissue response has been recognized as an important metric in biocompatibility testing [62]. During a normal wound healing response, cells and their products interact to repair damaged tissues. If an implant is present, these processes can be disrupted [63]. For this study, the bone in which the screw was inserted was considered the local

tissue. The soft tissue above the screw head was not histologically analyzed for biocompatibility. In future studies, all local tissues including the soft tissue surrounding the screw head will be analyzed for biocompatibility. The goal was to determine the basic host response and biocompatibility of the host material by characterizing the extent of inflammation, bone/screw resorption by osteoclasts, and bone deposition by osteoblasts.

To confirm biocompatibility and initiation of the remodeling process, the samples were prepared for histological staining using hematoxylin and eosin (H&E) and trichrome stains (Figure 32 – Figure 37). H&E stain uses hematoxylin to stain the nuclei of cells blue and eosin Y to stain other eosinophilic structures red, pink, or orange. Trichrome stain is a three-color staining protocol where muscle fibers and keratin are stained red, collagen and bone are stained blue, cytoplasm are stained red or pink, and cell nuclei are stained dark brown or black.

There was recruitment of osteoclasts and early resorption of the screw at the periphery, paired with early osteoblast deposition of osteoid. There was fibrin deposition surrounding the screws and between early bone remodeling units. Furthermore, there were osteoclasts with adjacent absorption of screw material and active osteoblasts with osteoid deposition. Although not quantifiable at this point, the early resorption of the screw material at 4 weeks *in vivo* shows signs of degradation due to surface erosion similar to the enzymatic degradation *in vitro*.

Figure 32 is a representative image of a silk screw in a rat femur. The conical screw head can be seen above the cortical bone and the screw threads are fixed in the bone. This image shows that there are boney units in between the threads of the bone as denoted by the solid pink color on the top left portion of the threads of the screw. After 4 weeks *in vivo*, it is difficult to say whether the screws cut the threads or if the bone is simply growing in between the threads. Nevertheless, it is a good sign that the screw does not simply look forced into the pilot hole but the bone is mirroring the thread profile of the screw. It should be noted that the tissue in histological images is often folded or pushed during sectioning. It can be stated with confidence that there are not large voids in the bone in this image but simply an artifact of histology.

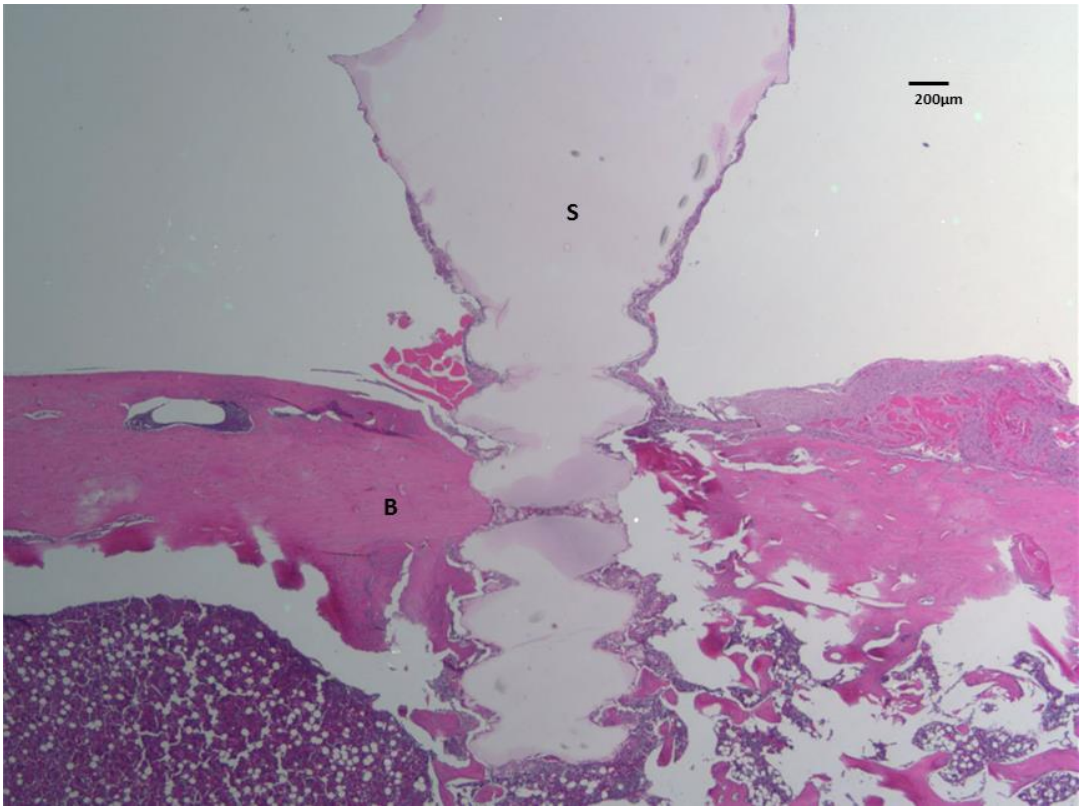

Figure 32 – Full perspective image of screw [S] fixed in bone [B] after 4 weeks *in vivo*.

Figure 33 depicts a trichrome stain of bone in between two threads of a silk screw. The screw is denoted by the solid pink color and the bone is denoted by the blue color. Minimal fibrin deposition can be seen at this stage. Fibrin deposition is usually associated with scar formation or clot so minimal amount of fibrin deposition after 4 weeks *in vivo* indicates that the bone is probably forming normally. The trichrome stain highlights the osteoclasts consuming the screw as well as osteoblasts depositing new bone around the screw. Both of these cell types and interactions are encouraging towards a normal bone remodeling process.

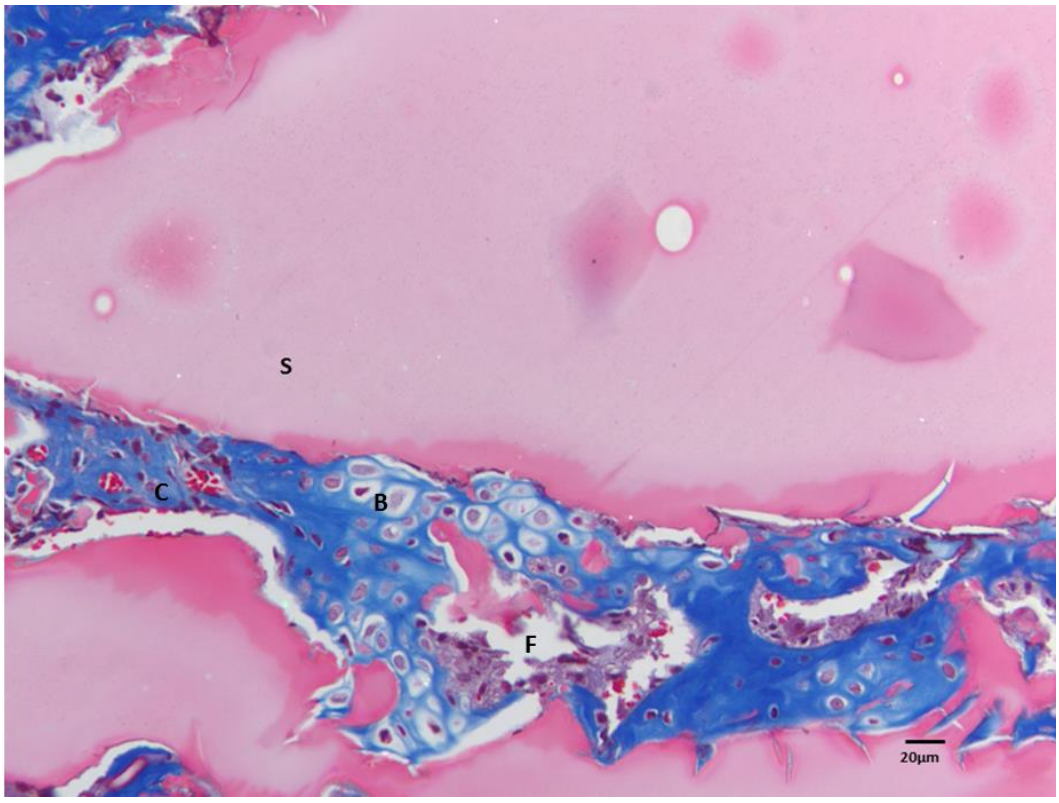

Figure 33 – Trichrome stain of screw in bone at 20X after 4 weeks *in vivo*. The trichrome stain highlights osteoclasts [C] consuming the screw [S], as well as osteoblasts [B] depositing new bone with minimal fibrin [F] deposition at this stage.

Figure 34 is an excellent example of the remodeling process and bone deposition. Osteoclasts (C) with adjacent resorption of screw material (S) can be seen at the

periphery of the screw material. Active osteoblasts can also been seen depositing osteoid (B). Osteoid is the unmineralized, organic portion of the bone matrix that has yet to undergo calcification. Osteoid deposition is a good sign after 4 weeks *in vivo* as the bone is showing signs of early remodeling units.

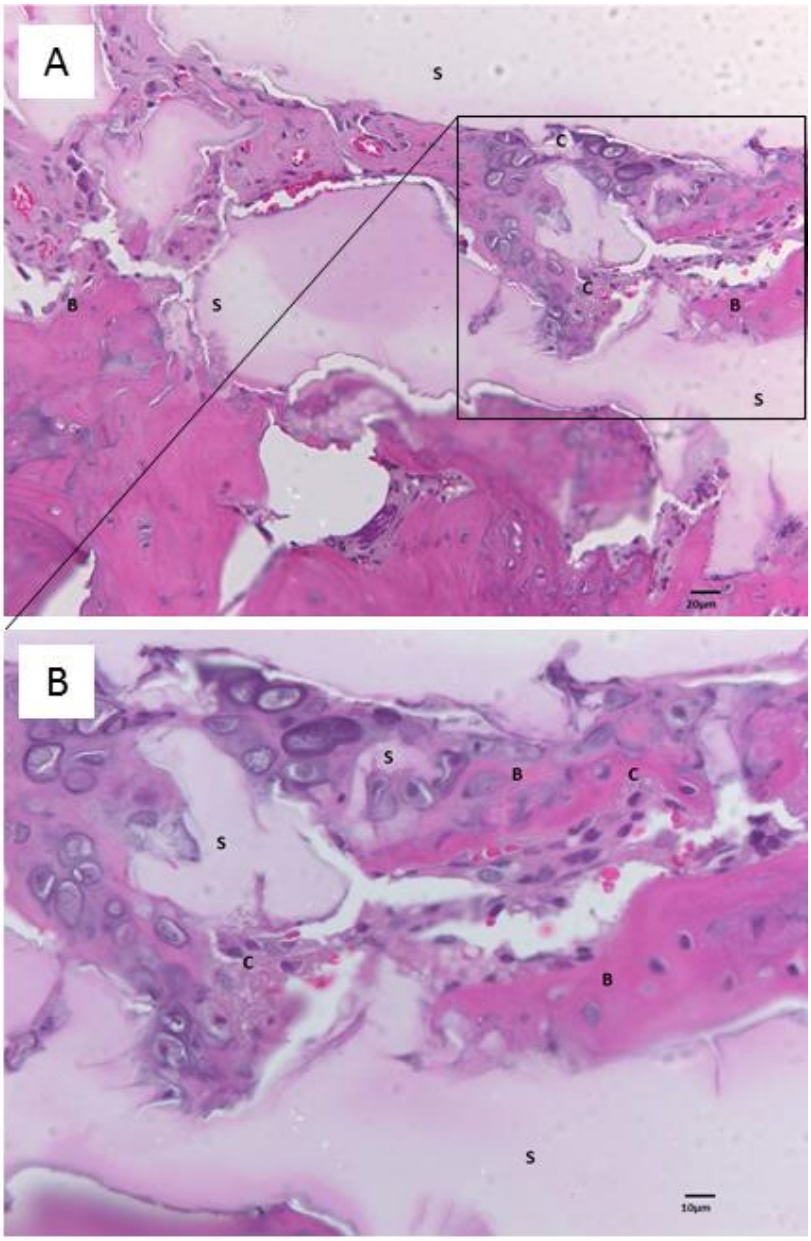

Figure 34 – H&E stain of silk screw in bone after 4 weeks *in vivo*. Osteoclasts [C] with adjacent absorption of screw material [S], and active osteoblasts with osteoid deposition [B]. (A) 20X. (B) 40X.

Figure 35 shows similar remodeling as depicted in Figure 33 and Figure 34 but on the outside edge of the screw threads. This image shows a close up interaction between osteoclasts and the screw threads at the interface of bone damage. In the top left portion of image A, with the labels (B) and (C) denoting osteoid deposition and osteoclasts respectively, it appears as if the screw threads initially protruded further into the bone and are now being consumed by the congregation of osteoclasts. Further, osteoblasts are depositing osteoid at this interface showing that the bone is properly remodeling as the screw degrades.

Figure 36 is a comprehensive image of both staining methods as well as a high magnification image of the remodeling process. In image C, osteoclasts can be seen resorbing silk material and osteoblasts are seen depositing osteoid. These are both good signs that the simultaneous remodeling process of breaking down damaged bone or removing material and reforming bone with osteoid deposition is occurring properly.

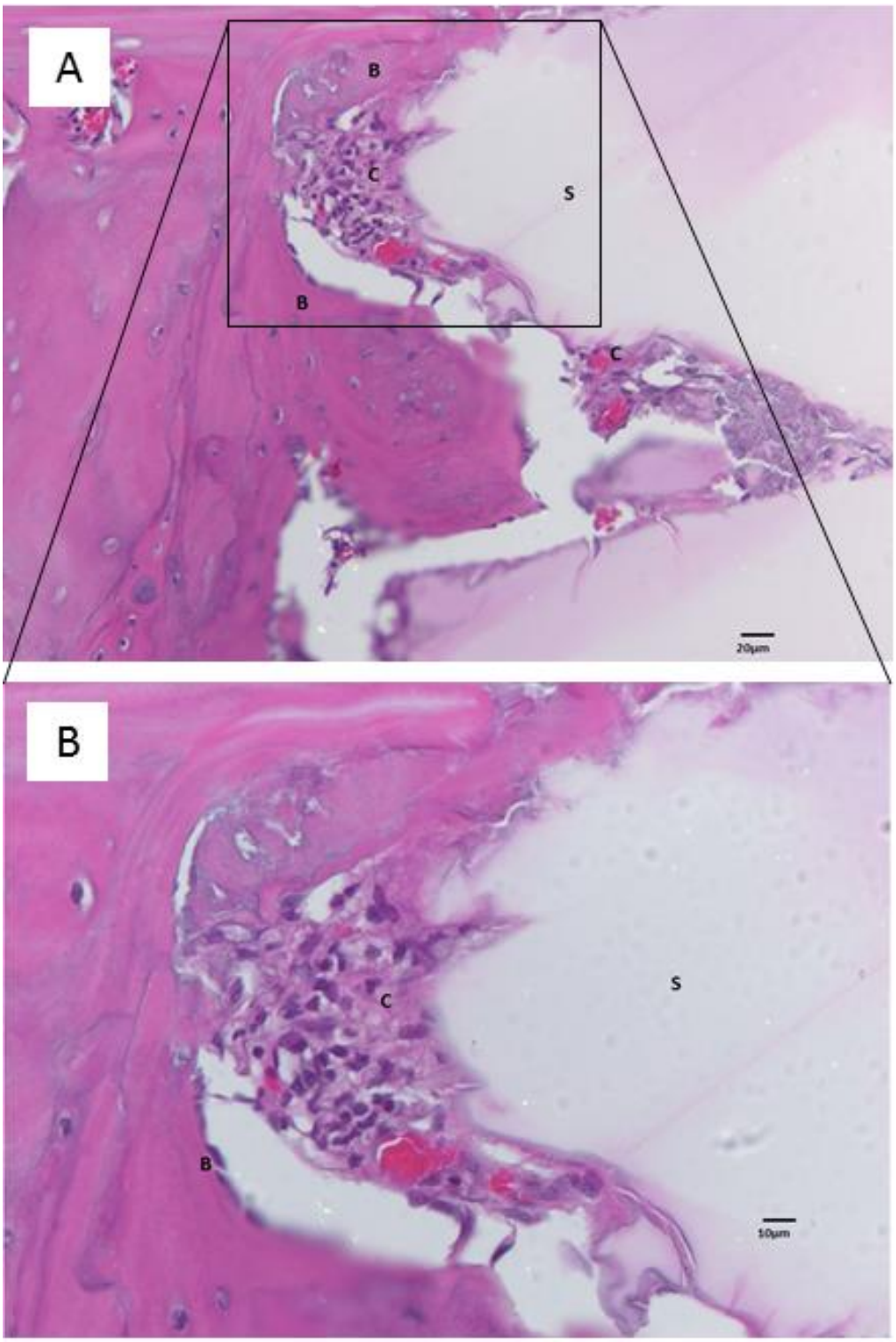

Figure 35 – H&E stain of screw in bone after 4 weeks *in vivo* shows the remodeling process occurring in between the threads of the silk screw. Osteoclasts [C] with adjacent absorption of screw material [S], and active osteoblasts with osteoid deposition [B]. (A) 20X. (B) 40X.

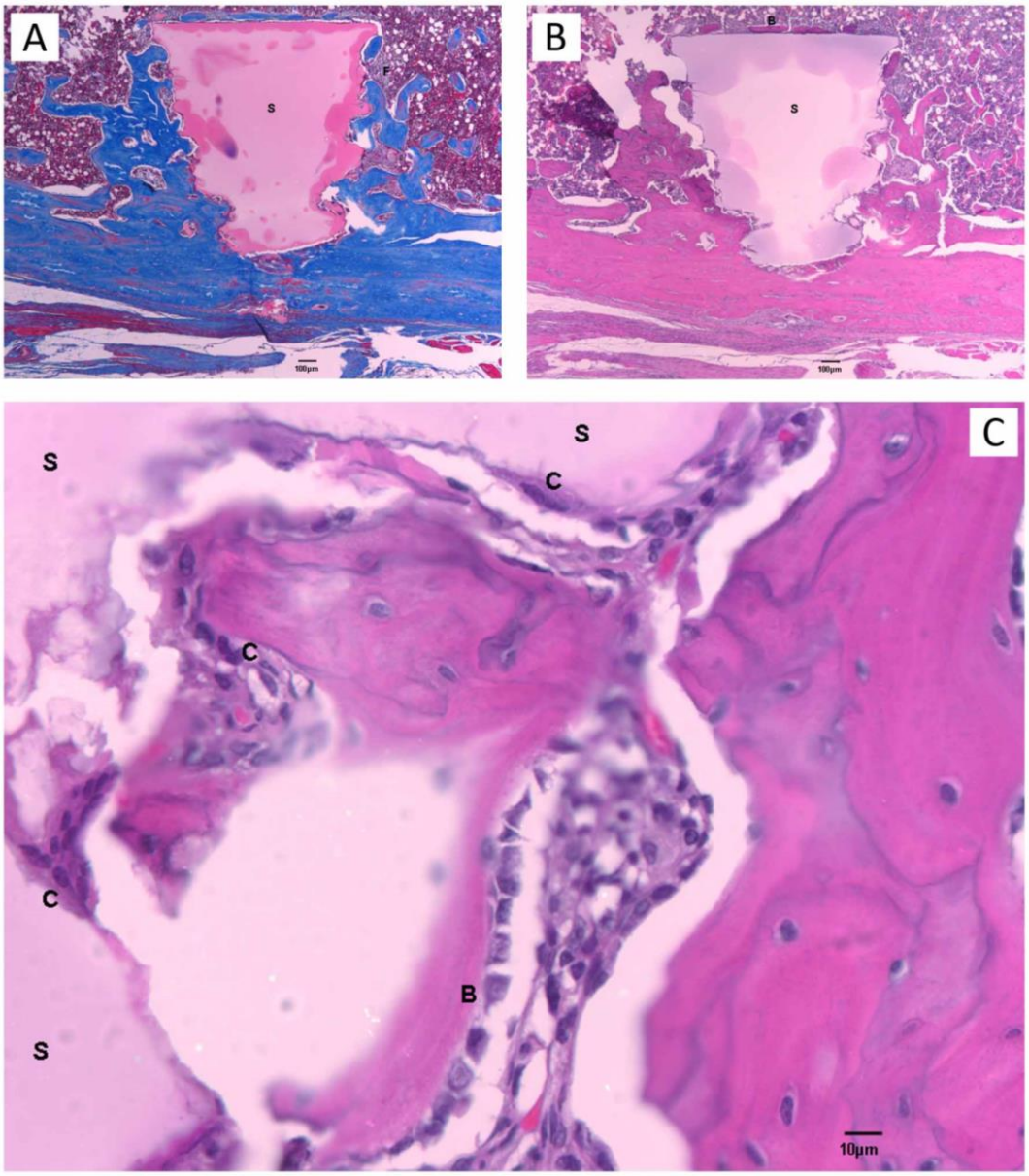

Figure 36 – Histological characterization of the silk screws after 4 weeks *in vivo*. (A) Trichrome stain at 4X power: fibrin deposition [F] surrounding the screw [S], and between early bone modeling units. (B) H&E stain: recruitment of osteoclasts and early resorption of the screw [S] at the periphery, paired with early osteoblast deposition of osteoid. Early formation of bone modeling units can be seen at 40X power [B]. (C) H&E stain at 40X: presence of osteoclasts [C] with adjacent absorption of screw material (S), and active osteoblasts with osteoid deposition (B).

4.10.3 Histology of subcutaneous plugs

Cylindrical plugs of the same material were implanted subcutaneously to confirm biocompatibility. The samples were prepared by histological sectioning to assess

implant-host interfaces. After one and four weeks *in vivo*, the loose connective tissue and subcutaneous adipose tissue adjacent to the implant contained infiltration of neutrophils (Figure 37). This region of neutrophil infiltration extended approximately 25 to 100 microns from the implant surface. Connective and adipose tissue outside this region exhibited moderate neutrophilic infiltration that increased in density with proximity to the implant. Acute mild inflammation was associated with the foreign body and no evidence of necrosis was found.

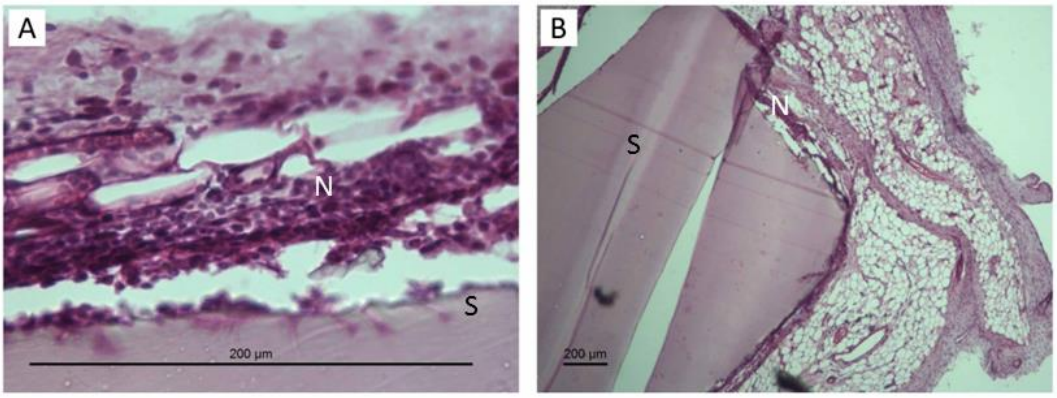

Figure 37 – Histology of subcutaneous implants after one week *in vivo*: moderate neutrophil infiltration [N]. The silk implant is the uniform shade of translucent purple [S]. (A) 40X magnification. (B) 4X magnification. Note: samples were damaged during microtome cutting as noted by the separation of silk from the neutrophil layer.

5. Discussion

5.1 Fabrication

The molding of the silk screw blanks was difficult due to the viscosity of the high concentration silk solutions. The viscosity did not permit uniform flow and settling of solution into the molds, resulting in weld lines when different flows met. Because HFIP is volatile and evaporates quickly, the molds could not be left in ambient conditions for extended periods of time to allow bubbles to migrate out of the solution. Therefore, it was necessary to place the molds in methanol soon after filling to prevent the air bubbles from escaping or the solution from completely settling. Therefore, roughly half of the blank could be used for machining while the other half was discarded due to non-cylindrical geometry or the presence of bubbles.

Using the uniform portion of the blanks, silk screws were easily manufactured using simple machining practices. The pure silk blanks were turned down to any major diameter with the lathe. In order to prevent deflection of the silk blanks and, thus, inconsistent diameters along the length of the blank, the blanks were turned slowly, while compressed air and vacuum were used to clear any debris from the cutting location. Once the correct major diameter was achieved using a basic screw size chart, a die was used to cut the threads into the silk blank. This process also worked better when performed slowly as less material would be removed causing the thread profile to be the same as standard metal screws. If the threads were cut too quickly, the major diameter was less than the standard size,

the shank of the screw would fracture, or the die would skip previously cut threads causing deformation and poor thread geometries. Also, the threads were often cut at an angle different from standard machine screws due to the inconsistency of turning a die by hand. While the thread profiles are not identical between different screws and do not mimic a bone screw thread profile, this study shows that screw and thread geometries can be manufactured using simple machining techniques. In the future, a bone screw die or thread whirling tool will be used to cut bone screw threads into the silk blanks.

Silk plates were molded similarly to the screw blanks but in larger rectangular molds. The portion of the plate that contacted the methanol initially often deformed significantly. The plates were prepared to the correct thickness using diamond sanding tools, sand paper, belt sanders, or a mill. Once the desired thickness was achieved, the plates were cut into different shapes using a razor blade or band saw. The plates were easier to cut when hydrated.

5.2 Mechanical and related material properties

The pure silk pins were consistent in terms of mechanical properties during dry double lap shear testing and achieved a maximum shear stress of 104 MPa. A residual load remained at the end of each test which was hypothesized to be from the dragging of the fractured shear plugs on the fixture. This had no impact on the resulting maximum shear stress of the test. PLGA screws composed of 82:18 or 80:20 PLA:PGA are reported to achieve a maximum shear stress of roughly 100

MPa [52, 57]. For the first material iteration of silk, a dry maximum shear stress of 104 MPa was comparable to the properties of PLGA. Further improvements can be made with the addition of silk micro-fibers [27] or silk micro-particles [64]. The limitations of the current silk format include hydrated mechanical strength, as strength significantly decreased when hydrated. Nevertheless, despite the ASTM standard's requirements of testing in a 100% hydrated environment, this does not mimic *in vivo* bone conditions. The inside and surface of the bone is not equivalent to an aqueous environment preventing the silk screws from losing strength in the presented *in vitro* mechanical studies. Future *in vivo* mechanical characterizations will be performed to test the hypothesis that silk screws retain significant strength *in vivo*. Further, as discussed in the background, the dry mechanical properties are far more important in non-load bearing applications such as CMF procedures due to mechanical stresses during implantation.

Pull-out strength tests were performed to determine 1) the maximum load and 2) the failure mode. In both dry and hydrated tests, the results were dependent on the major diameter of the screw. Larger major diameters achieved much greater loads. The sample with a significantly larger diameter than the rest of the samples (0.067 in; 1.69 mm), reached a load of 95.22 N which was above any other pull-out strength result; this sample pulled out of the bone block with no visible physical damage to the screw. This is expected as more material will be engaged with the bone block with a larger major diameter. For all dry tests, the screws pulled out of the bone block undamaged and it was hypothesized that the failure

mode was from the artificial bone, not the screw. For the hydrated tests, the failure mode was not as consistent as two screws fractured below the head and four screws pulled out of the artificial bone. Generally, the screws with the smaller major diameter pulled out of the bone while the screws with the larger major diameter fractured below the head. These data exemplify that consistent major diameters need to be generated in order to provide consistent test results as discussed above.

For non-load bearing applications such as CMF fixations, the non-hydrated mechanical properties are far more important than the hydrated properties. This is because the devices need to have sufficient strength to be implanted but require very minimal strength to fixate a non-load bearing fracture to allow for proper bone remodeling to begin. Thus, because the silk devices have significant non-hydrated mechanical properties and have been shown to be self-tapping, the non-hydrated mechanical properties are suitable for implantation of the screws. Further, as discussed in the background, the goal of the silk fixation devices was to have a similar implantation technique to metallic screws. Because the silk screws have been shown to be self-tapping, the screws can be implanted without the laborious and tedious step of pre-tapping the pilot hole as is the case with current resorbable devices. Thus, silk screws have an immediate benefit over current resorbable devices.

Autoclaved samples absorbed significantly less water than non-autoclaved samples most likely due to compaction of the silk which results in an increase in density of silk after autoclaving. Samples lost between 1% and 3% of their mass and dimensions after the first autoclave cycle signifying that the samples were not fully dry and the autoclave cycle was driving off excess water causing a resulting shrinkage. Samples were autoclaved a second time to determine the stability of the samples and they were dimensionally stable after this second cycle signifying that no shrinkage or deformation will occur post-machining.

Autoclaving also showed effects on the mechanical properties of the material. After 10 autoclave cycles, the shear stress decreased significantly from 104.21 MPa to 81.49 MPa ($p < 0.01$). While 10 cycle autoclaved samples may still be useful in the clinical setting, future tests need to be done to characterize the effect on other material properties after multiple autoclave cycles. For example, after 10 autoclave cycles, the shear strength may decrease but still be strong enough to be implanted and stabilize a fracture. However, the multiple autoclave cycles may degrade the molecular weight of the material resulting in a faster degradation. Because the degradation profile appears very slow, autoclaving may be used as a material optimization technique. Thus, future tests need to be performed to fully characterize the effect of autoclaving on the material such as enzymatic degradation and swellability.

5.3 In vivo characterization and implantation technique

While current resorbable devices provide many benefits, they present laborious implantation requirements. The screws were self-tapping in the rat femur and did not show any negative host response. Current PLGA screws require a two-step process of drilling then pre-tapping the hole, resulting in extra work for the surgeon. Silk screws were implanted identically to current fixation procedures where a pilot hole is drilled and a self-tapping screw inserted. These data support the use of silk screws in a clinical setting as the implantation technique is the same as that of metallic screws and the materials appear to be well tolerated and initiate the anticipated remodeling process. After a 4 week time point, there were signs of early resorption of the screw material by osteoclasts and osteoid deposition of osteoid. In order for new bone to form, the screw material needs to be broken down to create space. The preliminary histological characterization shows that the body is capable of resorbing the screw material while also depositing new bone units. Further, there is not a marked, abnormal inflammatory response but simply what one would see in normal bone remodeling.

Because the silk screws were self-tapping during the *in vivo* implantation experiments, the self-tapping capabilities were confirmed by other means including microhardness testing and implantation in other bones (cadaver rat femurs, polyurethane bone mimic, and a cadaver human skull). The hardness of the silk constructs was 40 kg/mm^2. This value compares favorably with the microhardness of bone that is typically reported to be anywhere from 40 to 60

kg/mm^2. This is beneficial for remodeling purposes as the screw material is neither too soft nor too hard as compared to bone; this may explain the fact that osteoclasts are seen surrounding and resorbing the screw material in the histological characterization. Cell behavior can be guided by substrate stiffness [65] so a screw with similar hardness, which is directly correlated to stiffness [49], may help maintain a normal remodeling process. In addition, a silk screw with microhardness similar to that of bone may be able to be a self-tapping screw. Hardness is defined by the resistance of a material to indentation so a harder material will indent a softer one. Due to the variability in hardness values of human bone, it cannot be stated as fact that the hardness of the silk screw is greater than or less than that of bone. Rather, the hardness of the silk material falls within the range of the hardness values reported for human bone in various locations.

Because hardness testing alone is not sufficient to prove that the silk screws were self-tapping, multiple different techniques were used to show the self-tapping capabilities of the silk screws. Implantation in polyurethane full skull model, rat cadaver femurs, and a human cadaver skull all showed potential for self-tapping silk screws. While the polyurethane full skull model and cadaver rat femurs were not sectioned to view any potential internal threads, the human cadaver skull was sectioned and the cross-section of the bone/screw interface showed threads cut into the bone. While this is encouraging with regard to the utility of silk screws as self-tapping resorbable screws, future tests need to be performed with bone screw

threads and proper head geometries. Bone screw threads are much different than machine screw threads with different load-bearing properties so the implantation technique needs to be further explored with proper bone screw geometries. Nevertheless, the fact that these screws were able to cut threads into the bone shows promise for the self-tapping capabilities of silk screws.

Future material iterations may involve the incorporation of enzymes directly into the screws that activate upon rehydration [33, 34, 66, 67] to encourage degradation or the incorporation of bioactive compounds such as BMP-2 to promote bone ingrowth [29-31]. These factors can be used to modulate healing and promote proper remodeling of the bone. Silk plates also showed utility in implantation feasibility *in vitro* as the application of water allowed malleability of the plates. Rather than having to pre-shape the plates to the exact curvature of the bone using heating pads, probes, or baths, as is the case with current resorbable devices, the plates conformed to the shape of the bone and held in place after the insertion of the screws. This eliminates unnecessary effort by the surgeon as the silk plates are able to actively adapt to the shape of the bone without heat treatment.

Subcutaneous plugs showed no abnormal host response after 1 and 4 weeks. The plugs did not migrate subcutaneously and did not elicit any negative host response. This was necessary as a second means of determining biocompatibility and host response because any negative response may not be noticed within the

femur. The plugs showed no visible signs of degradation. In the future, longer time points are needed to determine the host response after significant degradation and mass loss.

5.4 Summary of discussion

The silk screws and plates showed promising utility for bone fracture fixation due to the mechanical properties, ease of implantation such as the self-tapping nature of the screws, ability to be resterilized, and ability to degrade both *in vivo* and *in vitro*. However, improvements are necessary to surpass currently accepted fixation systems. First, the mechanical properties need to improve to be stronger PLGA but weaker than metallic devices to avoid stress shielding. The PLGA lacks sufficient strength and stiffness while the metal is too strong and can cause stress shielding of bone. Second, the screws and plates need to be tuned to degrade in a shorter time frame to allow for dynamic transfer of the load back to the healing bone. Both *in vitro* and *in vivo* degradation profiles of longer time points will be explored with the current material formulation to determine the baseline degradation profile. Third, the combination of the silk with bioactive compounds such as enzymes, bone morphogenetic protein 2 (BMP-2), and pharmaceuticals could provide multifunctional benefits not currently utilized in bone fixation systems. Since previous studies have demonstrated that the mechanical properties of silk can be significantly enhanced with micro-fibers and micro-particles, that the degradation rate can be controlled, and that the delivery

of bioactive compounds is possible, it is anticipated that the next versions of these silk screws and plates will address the needs outlined.

6. Conclusions

Conventional resorbable fixation devices provide benefits, however, they present laborious implantation requirements due to their poor mechanical properties and inability to be reused or resterilized. Silk screws were implanted identically to current metallic fixation procedures where a pilot hole is drilled and a self-tapping screw inserted. The silk screws were well tolerated and initiated the remodeling process anticipated. After a 4 week time point *in vivo*, there was minimal degradation of the silk screw. Silk plates also showed utility in implantation feasibility *in vitro* as the application of water allowed malleability of the plates. Rather than having to pre-shape the plates to the exact curvature of the bone, as is the case with current resorbable devices, the plates conformed to the shape of the bone and held in place after the insertion of the screws. This trait eliminates unnecessary effort by the surgeon as the silk plates are able to actively adapt to the shape of the bone without heat treatment, while maintaining the required mechanical support. Further, the hydrated mechanical properties may allow for better bone remodeling and flexibility for growing bones due to the decreased strength when hydrated. A flexible device may allow for mechanical signaling through micromotion of the devices which would promote better bone remodeling.

In the present study, the feasibility of silk as a molding and machinable biomaterial system for fixation devices was demonstrated. Silk has been utilized in formats for biomedical applications including sponges, fibers, foams, but not

previously as a solid, hard, compact material device. The silk material was easily machinable to different geometries and sizes allowing for flexibility in future designs. The silk screws and plates in this study exhibited comparative mechanical properties to resorbable PLGA materials, showed no negative host response, and remained fixed in the bone up to a 4 week time point. The screws were self-tapping eliminating the need for a two-step implantation process as is the case with current resorbable screws. The plates adapted to the curvature of the bone with the application of water and did not require a time-dependent heating step and pre-shaping. The versatility of silk protein will act as a benefit in future studies with future material iterations. Table 9 summarizes the current research on new silk fixation devices compared to well established metallic and resorbable devices. The disadvantages of using silk as a fracture fixation device are not fully explored but may include a limited application area, the silk may degrade too slowly, and the hydrated mechanicals may not be sufficient for fixation *in vivo*.

Table 9 – Summary table of current research on new silk fixation devices compared to current metallic and resorbable devices.

Type	Pros	Cons	Complication Rates	Application

Metallic	• Ease of implantation
	  • Self-tapping screws
	  • *In situ* plate shaping
	• Robust mechanical properties
	• Resterilization/reuse
		• Stress shielding
		• Temperature sensitivity
		• Plate exposure or migration
		• Corrosion
		• Growth disturbance in children
		• Palpability
		• Limited radiological imaging
		• Infection
			~ 10%	• All except pediatric CMF
				• Load bearing applications

Resorbable	• Improved bone remodeling and accelerated healing
	• Degradable device
	• Flexibility for growing bones
		• Laborious implantation technique
		  • Pre-drilling and tapping of hole
		  • Heat to shape plates
		• Degradation to acidic products
		• No resterilization/reuse
		• Inflammatory reaction
		• Sterile sinus formation
		• Osteolysis
			~ 6%	• Pediatric CMF
				• Non-load bearing applications

Silk	• Ease of implantation
	  • Self-tapping screws
	  • *In situ* plate shaping
	• Resterilization/reuse
	• Degradable device
	• Flexibility for growing bones (hydrated mechanicals)
		• Limited application area
		• Silk material may degrade too slowly
		• Hydrated mechanicals
		  • Too weak?
			N/A	• All CMF surgeries
				• Other applications with limited load bearing needs

7. Future Work

7.1 Continuation of work on silk screw and plate system

While the initial outcomes are promising, more material and physical characterizations of the silk screws and plates need to be performed. Long-term *in vivo* time points are necessary to evaluate long-term host response, bone remodeling, or onset of any complications during extended degradation of the screws and plates. The fabrication of silk plates needs to be optimized in order to obtain standard bone plate geometries such as plates with counter-sunk holes. A functional animal model fracture fixation will provide information on the capability of the silk screws and plates of adequately synthesizing a fracture despite the weakened hydrated mechanical properties. These models may include fixation of a critically sized femur defect or CMF fixation in a rat [68], mini-pig [69-71], or rabbit model [62, 72-74]. In addition, bone screws and plates need to be manufactured with bone threads and plate geometries identical to those currently used. The pull-out strength tests, implantation technique, and fixation potential in bone may change with different thread profiles. Other mechanical tests that are necessary to fully characterize the silk devices include torsional strength for screw insertion, and flexural stiffness for plates.

7.2 Enhancements to silk screw and plate system

With these successful outcomes with silk plates and screws, further enhancements can be envisioned in terms of mechanical properties. The silk solutions can be enhanced with silk particles or silk micro-fibers to produce a 100% silk composite

with improved mechanical properties [27, 64]. In some cases the screws and plates may also need to be tuned to degrade in a shorter time frame to allow for dynamic transfer of the load back to the healing bone. This could be accomplished numerous different ways such as autoclaving multiple times to degrade the silk fibroin or incorporating enzymes into the constructs that activate upon hydration [28, 33, 34]. Certain enzymes can be incorporated into the HFIP silk solutions so that they are stabilized in the silk material. Enzymes that will become inactive in HFIP or methanol may need to be coated on the surface of the screws then activated upon hydration.

Coating or loading the silk devices with bioactive compounds such as BMP-2 and other pharmaceuticals could provide benefits not successfully utilized in bone fixation systems at present. The devices could be dip-coated in bioactive compounds; or, because the devices swell significantly, certain compounds could be taken up by the silk devices after autoclaving in a sterile environment. The devices would then be dried, sterile packaged, then implanted *in vivo*. Such factors can be used to modulate healing and promote remodeling of bone. [29-31]

7.3 Exploration of other geometries and manufacturing techniques

Due to the success and versatility of a machinable silk process, other geometries and applications can be envisioned such as suture anchors, dental implants, Swanson prostheses, nasal reconstruction, and otoplasty. In addition, other machining techniques will be explored, including CNC machining, die cutting,

blanking, extruding, and chemical etching, to obtain more complex, intricate geometries. One interesting geometry that could be explored is a continuous, one-phase suture anchor. Because other research groups have made mechanically strong regenerated fibers from HFIP silk solutions [42, 43], the fibers could be chemically attached by redissolving part of the fiber in HFIP and attaching to the screw; also, the fiber and screw could be molded together and machined to the desired geometry.

Because implantation and post-surgical imaging of current resorbable fixation devices is a problem, the silk constructs could be enhanced with iron particles. The iron particles may aid the surgeon during implantation due to a magnetic screw that may be attracted to a screw driver. Further, once the surgery is complete, the surgeon could quickly check that all components are properly placed and have not migrated or failed with a simple magnetic sensor. This would allow for a first pass check of surgical errors and allow the surgeon to reopen the wound and fix the problem before the patient leaves the operating room. This would save on time, money, and recovery time.

References

1. Gilardino, M.S., E. Chen, and S.P. Bartlett, *Choice of Internal Rigid Fixation Materials in the Treatment of Facial Fractures*. Craniomaxillofacial Trauma & Reconstruction, 2009. **2**(1): p. 49.
2. Neumann, A. and K. Kevenhoerster, *Biomaterials for craniofacial reconstruction*. GMS Current Topics in Otorhinolaryngology, Head and Neck Surgery, 2009. **8**.
3. *2012 Reconstructive Plastic Surgery Statistics*, in *American Society of Plastic Surgeons*2013, ASPS Public Relations.
4. Verleyen, K., D. Brown, and M. Hussey. *US Markets For Trauma Devices 2012*. 2011 [cited 2011 June 13]; Available from: http://mrg.net/Products-and-Services/Syndicated-Report.aspx?r=rpus21tr11.
5. Adelson, R.T., R.J. DeFatta, and Y. Ducic, *Integrity of craniofacial plating systems after multiple sterilization procedures*. Journal of Oral and Maxillofacial Surgery, 2007. **65**(5): p. 940-944.
6. Goldberg, D.S., et al., *Critical review of microfixation in pediatric craniofacial surgery*. Journal of Craniofacial Surgery, 1995. **6**(4): p. 301.
7. Simon, J.A., J.L. Ricci, and P.E. Di Cesare, *Bioresorbable fracture fixation in orthopedics: a comprehensive review. Part I. Basic science and preclinical studies*. Am J Orthop (Belle Mead NJ), 1997. **26**(10): p. 665-71.
8. Zhang, J., et al., *A Comparison of Absorbable Screws and Metallic Plates in Treating Calcaneal Fractures: A Prospective Randomized Trial*. J Trauma, 2011.
9. Eppley, B.L., *Use of resorbable plates and screws in pediatric facial fractures*. Journal of oral and maxillofacial surgery: official journal of the American Association of Oral and Maxillofacial Surgeons, 2005. **63**(3): p. 385.
10. Imola, M.J., et al., *Resorbable Plate Fixation in Pediatric Craniofacial Surgery Long-term Outcome*. Archives of Facial Plastic Surgery, 2001. **3**(2): p. 79-90.
11. Pietrzak, W., D. Sarver, and D. Kohn, *Fatigue testing of bioabsorbable screws in a synthetic bone substrate*. Mechanical Testing of Bone and the Bone-Implant Interface, CRC Press, New York, 2000: p. 581-592.
12. Larsen, M.W., W.S. Pietrzak, and J.C. DeLee, *Fixation of osteochondritis dissecans lesions using poly (l-lactic acid)/poly (glycolic acid) copolymer bioabsorbable screws*. The American journal of sports medicine, 2005. **33**(1): p. 68-76.
13. Iizuka, T. and C. Lindqvist, *Rigid internal fixation of mandibular fractures: an analysis of 270 fractures treated using the AO/ASIF method*. International journal of oral and maxillofacial surgery, 1992. **21**(2): p. 65-69.
14. Paavolainen, P., et al., *Effect of rigid plate fixation on structure and mineral content of cortical bone*. Clinical Orthopaedics and Related Research, 1978. **136**: p. 287.
15. Bos, R.R., et al., *Resorbable poly (L-lactide) plates and screws for the fixation of zygomatic fractures*. Journal of Oral and Maxillofacial Surgery, 1987. **45**(9): p. 751-753.
16. Böstman, O., et al., *Tissue restoration after resorption of polyglycolide and poly-laevo-lactic acid screws*. Journal of Bone & Joint Surgery, British Volume, 2005. **87**(11): p. 1575-1580.
17. Dumont, C., et al., *Clinical results of absorbable plates for displaced metacarpal fractures*. The Journal of hand surgery, 2007. **32**(4): p. 491-496.

18. Simon, J.A., J.L. Ricci, and P.E. Di Cesare, *Bioresorbable fracture fixation in orthopedics: a comprehensive review. Part II. Clinical studies.* Am J Orthop (Belle Mead NJ), 1997. **26**(11): p. 754-62.
19. Bostman, O.M., *Absorbable implants for the fixation of fractures.* J Bone Joint Surg Am, 1991. **73**(1): p. 148-53.
20. Bozic, K.J., et al., *Mechanical testing of bioresorbable implants for use in metacarpal fracture fixation.* The Journal of hand surgery, 2001. **26**(4): p. 755-761.
21. Waris, E., et al., *Bioabsorbable miniplating versus metallic fixation for metacarpal fractures.* Clinical Orthopaedics and Related Research, 2003. **410**: p. 310.
22. Lionelli, G.T. and R.A. Korentager, *Biomechanical failure of metacarpal fracture resorbable plate fixation.* Annals of plastic surgery, 2002. **49**(2): p. 202-206.
23. Bostman, O., *Osteolytic changes accompanying degradation of absorbable fracture fixation implants.* Journal of Bone & Joint Surgery, British Volume, 1991. **73**(4): p. 679-682.
24. Rockwood, D.N., et al., *Materials fabrication from Bombyx mori silk fibroin.* Nature protocols, 2011. **6**(10): p. 1612-1631.
25. Lefèvre, T., M.-E. Rousseau, and M. Pézolet, *Protein secondary structure and orientation in silk as revealed by Raman spectromicroscopy.* Biophysical Journal, 2007. **92**(8): p. 2885-2895.
26. Wang, Y., et al., *< i> In vivo </i> degradation of three-dimensional silk fibroin scaffolds.* Biomaterials, 2008. **29**(24): p. 3415-3428.
27. Mandal, B.B., et al., *High-strength silk protein scaffolds for bone repair.* Proceedings of the National Academy of Sciences, 2012. **109**(20): p. 7699-7704.
28. Pritchard, E.M., et al., *Incorporation of proteinase inhibitors into silk-based delivery devices for enhanced control of degradation and drug release.* Biomaterials, 2011. **32**(3): p. 909-918.
29. Karageorgiou, V., et al., *Bone morphogenetic protein-2 decorated silk fibroin films induce osteogenic differentiation of human bone marrow stromal cells.* Journal of Biomedical Materials Research Part A, 2004. **71**(3): p. 528-537.
30. Karageorgiou, V., et al., *Porous silk fibroin 3-D scaffolds for delivery of bone morphogenetic protein-2 in vitro and in vivo.* Journal of Biomedical Materials Research Part A, 2006. **78**(2): p. 324-334.
31. Li, C., et al., *Electrospun silk-BMP-2 scaffolds for bone tissue engineering.* Biomaterials, 2006. **27**(16): p. 3115-3124.
32. Wang, X., et al., *Controlled release from multilayer silk biomaterial coatings to modulate vascular cell responses.* Biomaterials, 2008. **29**(7): p. 894-903.
33. Lu, Q., et al., *Stabilization and release of enzymes from silk films.* Macromolecular bioscience, 2010. **10**(4): p. 359-368.
34. Lu, S., et al., *Stabilization of enzymes in silk films.* Biomacromolecules, 2009. **10**(5): p. 1032-1042.
35. Altman, G.H., et al., *Silk-based biomaterials.* Biomaterials, 2003. **24**(3): p. 401-416.
36. Vepari, C. and D.L. Kaplan, *Silk as a biomaterial.* Progress in polymer science, 2007. **32**(8): p. 991-1007.
37. Jin, H.-J., et al., *Bioprocessing of silk proteins-controlling assembly.* Bionanotechnology, 2006: p. 189-208.

38. Lotz, B. and F. Colonna Cesari, *The chemical structure and the crystalline structures of< i> Bombyx mori</i> silk fibroin*. Biochimie, 1979. **61**(2): p. 205-214.
39. Tsuboi, Y., et al., *Light can transform the secondary structure of silk protein*. Applied Physics A: Materials Science & Processing, 2001. **73**(5): p. 637-640.
40. Roccatano, D., et al., *Effect of hexafluoroisopropanol alcohol on the structure of melittin: A molecular dynamics simulation study*. Protein science, 2009. **14**(10): p. 2582-2589.
41. Hirota, N., Y. Goto, and K. Mizuno, *Cooperative α-helix formation of β-lactoglobulin and melittin induced by hexafluoroisopropanol*. Protein science, 1997. **6**(2): p. 416-421.
42. Zhao, C., et al., *Structural characterization and artificial fiber formation of Bombyx mori silk fibroin in hexafluoro-iso-propanol solvent system*. Biopolymers, 2003. **69**(2): p. 253-259.
43. Zhu, Z., K. Ohgo, and T. Asakura, *Preparation and characterization of regenerated Bombyx mori silk fibroin fiber with high strength*. eXPRESS Polymer Lett, 2008. **2**: p. 885-889.
44. Rho, J.-Y., L. Kuhn-Spearing, and P. Zioupos, *Mechanical properties and the hierarchical structure of bone*. Medical engineering & physics, 1998. **20**(2): p. 92-102.
45. Boivin, G., et al., *The role of mineralization and organic matrix in the microhardness of bone tissue from controls and osteoporotic patients*. Bone, 2008. **43**(3): p. 532-538.
46. Manolagas, S.C. and R.L. Jilka, *Bone marrow, cytokines, and bone remodeling. Emerging insights into the pathophysiology of osteoporosis*. The New England journal of medicine, 1995. **332**(5): p. 305.
47. Schindeler, A., et al. *Bone remodeling during fracture repair: the cellular picture*. in *Seminars in cell & developmental biology*. 2008. Elsevier.
48. Evans, G., et al., *Microhardness and Young's modulus in cortical bone exhibiting a wide range of mineral volume fractions, and in a bone analogue*. Journal of Materials Science: Materials in Medicine, 1990. **1**(1): p. 38-43.
49. Zysset, P.K., et al., *Elastic modulus and hardness of cortical and trabecular bone lamellae measured by nanoindentation in the human femur*. Journal of biomechanics, 1999. **32**(10): p. 1005-1012.
50. WEAVER, J.K., *The microscopic hardness of bone*. The Journal of Bone & Joint Surgery, 1966. **48**(2): p. 273-288.
51. Hu, X., D. Kaplan, and P. Cebe, *Determining beta-sheet crystallinity in fibrous proteins by thermal analysis and infrared spectroscopy*. Macromolecules, 2006. **39**(18): p. 6161-6170.
52. Pietrzak, W.S., D.S. Caminear, and S.V. Perns, *Mechanical characteristics of an absorbable copolymer internal fixation pin*. The Journal of foot and ankle surgery, 2002. **41**(6): p. 379-388.
53. Numata, K., P. Cebe, and D.L. Kaplan, *Mechanism of enzymatic degradation of beta-sheet crystals*. Biomaterials, 2010. **31**(10): p. 2926-2933.
54. Horan, R.L., et al., *In vitro degradation of silk fibroin*. Biomaterials, 2005. **26**(17): p. 3385-3393.
55. Wang, L., R. Nemoto, and M. Senna, *Three-dimensional porous network structure developed in hydroxyapatite-based nanocomposites containing enzyme pretreated silk fibroin*. Journal of Nanoparticle Research, 2004. **6**(1): p. 91-98.
56. Ziv, V., H. Wagner, and S. Weiner, *Microstructure-microhardness relations in parallel-fibered and lamellar bone*. Bone, 1996. **18**(5): p. 417-428.

57. Mäkinen, T., et al., *Efficacy of bioabsorbable antibiotic containing bone screw in the prevention of biomaterial-related infection due to< i> Staphylococcus aureus</i>*. Bone, 2005. **36**(2): p. 292-299.
58. Tweedie, C.A. and K.J. Van Vliet, *On the indentation recovery and fleeting hardness of polymers*. Journal of materials research, 2006. **21**(12): p. 3029-3036.
59. Burstein, A.H., D.T. Reilly, and M. Martens, *Aging of bone tissue: mechanical properties*. The Journal of bone and joint surgery. American volume, 1976. **58**(1): p. 82.
60. McCalden, R., J. McGeough, and M. Barker, *Age-related changes in the tensile properties of cortical bone. The relative importance of changes in porosity, mineralization, and microstructure*. The Journal of bone and joint surgery. American volume, 1993. **75**(8): p. 1193.
61. Bembey, A., et al., *Hydration effects on the micro-mechanical properties of bone*. Journal of materials research, 2006. **21**(08): p. 1962-1968.
62. Tiainen, J., et al., *Self-reinforced polylactide/polyglycolide 80/20 screws take more than 1½ years to resorb in rabbit cranial bone*. Journal of Biomedical Materials Research Part B: Applied Biomaterials, 2004. **70**(1): p. 49-55.
63. Vince, D.G., J.A. Hunt, and D.F. Williams, *Quantitative assessment of the tissue response to implanted biomaterials*. Biomaterials, 1991. **12**(8): p. 731-736.
64. Rajkhowa, R., et al., *Reinforcing silk scaffolds with silk particles*. Macromolecular bioscience, 2010. **10**(6): p. 599-611.
65. Lo, C.-M., et al., *Cell movement is guided by the rigidity of the substrate*. Biophysical Journal, 2000. **79**(1): p. 144-152.
66. Zhang, J., et al., *Stabilization of vaccines and antibiotics in silk and eliminating the cold chain*. Proceedings of the National Academy of Sciences, 2012. **109**(30): p. 11981-11986.
67. Numata, K. and D.L. Kaplan, *Silk-based delivery systems of bioactive molecules*. Advanced drug delivery reviews, 2010. **62**(15): p. 1497-1508.
68. Viljanen, J.T., et al., *Comparison of the tissue response to absorbable self-reinforced polylactide screws and metallic screws in the fixation of cancellous bone osteotomies: An experimental study on the rabbit distal femur*. Journal of orthopaedic research, 1997. **15**(3): p. 398-407.
69. Springer, I.N.G., et al., *Craniectomy and noggin application in an infant model*. Journal of Cranio-Maxillofacial Surgery, 2007. **35**(3): p. 177-184.
70. Schön, R., et al., *Tissue reaction around miniplates used for the fixation of vascularized iliac crest bone grafts*. Oral Surgery, Oral Medicine, Oral Pathology, Oral Radiology, and Endodontology, 1997. **83**(4): p. 433-440.
71. Heidemann, W., H. Terheyden, and K. Louis Gerlach, *Analysis of the osseous/metal interface of drill free screws and self-tapping screws*. Journal of Cranio-Maxillofacial Surgery, 2001. **29**(2): p. 69-74.
72. Kellman, R.M., et al., *Bioresorbable screws for facial bone reconstruction: a pilot study in rabbits*. The Laryngoscope, 1994. **104**(5): p. 556-561.
73. Tiainen, J., et al., *Bone tissue concentrations of ciprofloxacin released from biodegradable screws implanted in rabbits skull*. European journal of plastic surgery, 2012. **35**(2): p. 171-175.
74. Päivärinta, U., et al., *Intraosseous cellular response to biodegradable fracture fixation screws made of polyglycolide or polylactide*. Archives of orthopaedic and trauma surgery, 1993. **112**(2): p. 71-74.